Article:
Herterich, J, Richardson, I orcid.org/0000-0002-4340-7121, Moro, F et al. (2 more authors) (2022) Microstructure and Phase Assemblage of Low-Clinker Cements during the Early Stages of Carbonation. Cement and Concrete Research, 152. 106643. ISSN 0008-8846

https://doi.org/10.1016/j.cemconres.2021.106643

Microstructure and Phase Assemblage of Low-Clinker Cements during the Early Stages of Carbonation

Julia Herterich[a], Ian Richardson[a], Fabrizio Moro[b], Maurizio Marchi[c], Leon Black[a]*

[a] School of Civil Engineering, University of Leeds, Woodhouse Lane, Leeds LS2 9JT, UK

[b] LafargeHolcim Research Centre, 95, rue du Montmurier, BP 15 38291 Saint-Quentin Fallavier, France

[c] Global Product Innovation – HeidelbergCement Group, i.Lab, 87, Via Stezzan0, 24126, Bergamo, Italy

*Corresponding author. Tel.: + 44 113 343 2283. E-mail address: l.black@leeds.ac.uk

Abstract

Blending Portland cement with fly ash or ground granulated blast furnace slag effectively reduces its carbon footprint. However, these materials hydrate more slowly than Portland cement. Therefore, their early-stage behaviour is of interest.

Fly ash- and slag-containing cement pastes were cured for 72 hours and 28 days before exposure to ambient air (ca. 400ppm). Changes in carbonation behaviour at 0%, 30% and 60% replacement and w/b ratios (0.40 & 0.57) were studied. All Ca-bearing hydrate phases carbonated, but portlandite effectively buffered carbonation of other phases. Complete portlandite consumption permitted decalcification of the other phases, with substantial removal of Ca and Al from C-S-H and increased silicate polymerisation. When portlandite was present, monosulfoaluminate transformed to hemi- and monocarboaluminate, but complete decalcification only occurred when portlandite was no longer available. Reduced w/b ratios improved carbonation resistance for materials with moderate substitution but couldn't mitigate the effects of high replacement levels.

Keywords: Carbonation (C), Curing (A), Blended cement (D), Microstructure (B), Characterization (B)

1. Introduction

The use of composite cements has become standard practice in the cement industry, addressing carbon emissions while improving material performance via microstructure enhancement [1, 2]. Partial replacement of Portland cement by pulverised fuel ash (PFA) and ground granulated blast furnace slag (GGBS) can improve durability by reducing diffusion and permeability [3-6]. However, the slower hydration rates of these materials necessitate good curing for these improvements to be seen, with greater permeability and porosity observed during early stages of curing [3-5, 7]. Although the need for appropriate curing procedures is recognised in British concrete standards, (BS EN 13670:2009) [8], there are huge variations in prescribed curing times in international standards, with curing periods for composite cements ranging from several hours to several months [8-11]. There are also examples in the literature [8, 12, 13] highlighting the adverse effects of inadequate curing on composite cements.

PFA hydrates minimally over the first 7 days of curing [14, 15], with GGBS reacting only slightly more [16]. Thus, failure to adhere to curing guidelines, e.g. by early formwork removal, may adversely affect material performance, exposing underdeveloped microstructures that are susceptible to ingress and attack from aggressive species.

Composite cements present additional limitations when considering carbonation resistance. Atmospheric CO_2 dissolves in pore solutions forming carbonic acid and reacting with Ca-bearing hydrate phases, producing $CaCO_3$. Portlandite initially reacts with carbonic acid much faster than does C-S-H [17-20]. Eventual passivation of portlandite crystals due to formation of a microcrystalline $CaCO_3$ layer inhibits further dissolution, preventing continued buffering of the pore solution. C-S-H's much larger reactive surface makes it far less

susceptible to formation of an impermeable layer, resulting in its continued reaction [17-19, 21, 22]. Composite cements' decreased portlandite contents [23-26] reduce the capability to chemically resist carbonation, and carbonation resistance correlates to initial portlandite [21, 22] and cement [13] contents. Furthermore, the potential of composite materials to limit CO_2 diffusion and ingress through microstructure refinement is lost following short curing periods. For ideally cured systems, both reaction kinetics and CO_2 diffusion play key roles, but as porosity increases, carbonation resistance becomes reliant on the chemical kinetics. This may have implications for improperly cured composite materials where reduced portlandite contents and open microstructures may permit continuous CO_2 replacement.

The effect of carbonation on phase assemblages and microstructures of composite cements following short periods of curing is not well understood. Many studies [17-21, 27-30] focus on mature systems with accelerated carbonation via elevated CO_2 concentrations. Modifications in carbonation behaviour exist between natural and accelerated conditions [17, 27] (although 3% CO_2 correlates well with atmospheric levels [27]) and are expected for immature microstructures where carbonation reactions may be principally controlled by kinetics. The present work attempts therefore to overcome these problems by examining the early age carbonation (up to 7 days) of cement pastes cured for 72 hours or 28 days, studying carbonation behaviour under ambient CO_2 levels, of PFA- and GGBS-containing cements at moderate (30%) and high (60%) replacement, and low (0.40) and high (0.57) w/b ratios. Extensive carbonation without recourse to elevated CO_2 levels has been achieved by using very thin specimens.

2. Materials and methods

2.1 Materials

A limestone-free CEM I 52.5R cement, a PFA with low Fe content* and a GGBS with good chemical reactivity were used throughout this study. The elemental composition of each material, as determined by x-ray fluorescence (XRF) analysis, is presented in Table 1, together with material densities, median particle diameters and slag basicity ratios. Table 2 shows the cement mineralogy. A small quantity of arcanite (K_2SO_4) was detected.

Table 1: Elemental composition of materials determined by XRF analysis, density measurements, particle size (d50) and GGBS basicity ratios.

		CEM I 52.5R	PFA	GGBS
Loss on Ignition	%	1.50		2.35
SiO_2	%	20.50	70.83	35.71
Al_2O_3	%	4.60	24.36	10.65
Fe_2O_3	%	2.40	2.24	0.45
TiO_2	%	0.30	1.48	0.73
MnO	%	0.00	0.05	0.23
CaO	%	63.40	0.06	43.32
MgO	%	2.00	0.23	3.97
SO_3	%	3.60		3.06
K_2O	%	0.74	0.64	0.45
Na_2O	%	0.13	0.10	0.16
P_2O_5	%	0.30	0.05	0.02
Total	%	99.47	100.04	101.09
Density	g/cm^3	3.17	2.33	2.94
d50	µm	11.7	23.6	7.4

Basicity ratios	Requirement	
CaO/SiO_2	>1.0	1.21
$CaO+MgO/SiO_2$	>1.0	1.32
$CaO+MgO/SiO_2+Al_2O_3$	1.0 – 1.30	1.02
$CaO+0.56Al_2O_3+1.4MgO/SiO_2$	>1.65	1.54
$CaO+MgO+Al_2O_3/SiO_2$	>1.0	1.62

Table 2: Phase content of CEM I 52.5R

		C_3S	C_2S	C_3A	C_4AF	Gypsum	Bassanite	Other
CEM I 52.5R	%	59	21	2.5	11	2.5	1	3

* The low iron content prevents NMR line broadening due to the presence of paramagnetic material.

2.2 Methods

Four paste systems (CEM I, CEM I with 30 vol% PFA, 30 vol% GGBS and 60 vol% GGBS) were studied. Composite materials were blended in a 5 litre roller ball mill for 2 hours, filling the vessel about one third full of cement and one third full of graded polypropylene balls (three hundred and eighty 12.7mm, one hundred and seventeen 19mm and sixty nine 25.4mm). Samples were cured for a short time (t_0) of 72 hours. This allowed the systems to develop enough strength to allow sample preparation while still representing an immature system. Samples were also cured for 28 days to observe differences between immature and mature samples. The paste samples were cast (w/b 0.40 or 0.57) and sealed in small plastic vials (ø = 12 mm, h = 47 mm) in a CO_2 free (<30 ppm) atmosphere and rotated for 24 hours (to prevent bleeding) at 22º +/-2ºC, before being vacuum sealed in plastic bags and cured in a water bath at 20ºC (+/- 2ºC). Following the required curing time, the hardened paste samples were cut into 0.5 mm slices and conditioned either in ambient air (~400 ppm CO_2, approx. 24ºC) or in a CO_2-free sample chamber. The use of thin slices allowed the study to focus on reaction kinetics, reducing the impact of porosity and transport properties. All samples were conditioned at 72.6% RH [16] (using a saturated KNO_3 – NH_4Cl solution) and ambient laboratory temperature (21-24ºC) for up to 7 days. Samples were characterised at t_0 and then after 1, 2, 4, and 7 days.

Samples were hydration stopped in a glove box under a CO_2-free atmosphere using isopropanol, with a minimum solvent to sample volume ratio of 300 and a 2 hour exchange period (determined based on sample dimensions and diffusivity[31]). The samples were subjected to secondary solvent replacement using diethyl ether (washed 3 times) before heating on a hotplate at 44ºC for 10 minutes. Samples were then stored in a vacuum desiccator with silica gel until characterisation.

Portlandite and $CaCO_3$ contents were calculated from thermogravimetric analysis. Samples were ground to a fine powder and heated from 20-1000ºC (15-18mg sample/platinum crucible) on a Stanton Redcroft Simultaneous Thermal Analyser STA 780 under a N_2

atmosphere at a heating rate of 10°C/minute. Weight losses associated with portlandite dehydration and the decarbonation of $CaCO_3$ were measured using the tangent method with inflection points on the DTA curve used to identify the region of mass loss. Phase contents were then normalised to dry weight (mass of sample at 1000°C).

For quantitative XRD analysis, samples were crushed to fine powders in an agate pestle and mortar. Since sample drying can affect the decomposition of AFt and the AFm phases [32], XRD analysis was performed on non-hydration stopped samples. Powders were backloaded into sample holders and diffraction patterns collected with a Bruker D2 Phaser with a 141mm goniometer radius operated at 30kV and 10mA equipped with CuKα radiation source. A LYNXEYE linear position sensitive detector was used to collect data over an angular range of 5° – 70° 2θ with a 0.034 ° step size, a dwell time of 2 seconds and a continuous rotation of 15 rotations/min. Rietveld refinement was performed using Topas Academic 4.2 software and the external standard method, with corundum as the reference material. Reference structure files were exported from ICSD (Inorganic Crystal Structure Database).

ATR-FTIR spectroscopy was performed on powdered, hydration-stopped samples using a Thermo Scientific Nicolet Is10 spectrometer, fitted with a Thermo Scientific Smart Diamond ATR sampling accessory over a wavenumber range of 400 - 4000cm^{-1}.

Analytical transmission electron microscopy (TEM) data was collected on ion-beam milled samples using a FEI Tecnai F20 200 kV FEG TEM fitted with a Gatan Orius SC600 CCD camera and an Oxford Instruments 80mm^2 SDD EDX detector running INCA software. Copper grids were glued to both sides of hand-thinned sections (~30µm thick) and argon ion beam milled with a 4° milling angle to prevent damage due to thermal effects. EDX data collected from C-S-H were checked by selected area electron diffraction (SAED) to be free from intermixing with microcrystalline phases prior to analysis.

^{29}Si MAS MNR spectra were obtained at the EPSRC UK National Solid-State NMR service at Durham University. Powdered, hydration stopped samples were sent to the NMR facility in sealed bags. Direct excitation ^{29}Si NMR experiments were performed on a Varian VNMRS

400 spectrometer with a 6mm rotor using a tetramethylsilane reference standard. The direct excitation used a pulse duration of 4.0µs and a spin rate of 6000Hz. A 30mS acquisition time, a 10 second recycle time and between 5000-6000 repetitions were used for each of the samples.

^{29}Si NMR spectral deconvolutions were performed using a user-made procedure for Igor Pro (WaveMetrics) as developed by Love and Brough [34] from which mean aluminosilicate chain lengths (MCL) and Al/Si ratios were calculated (details are provided in the supplementary material).

3. Results

3.1 Characterisation of t_0 samples

3.1.1 Degree of reaction

The degree of hydration was followed by monitoring portlandite contents. Portlandite contents determined by TGA and XRD were similar, with thermal analysis often giving slightly higher values, perhaps reflecting the formation of poorly crystalline portlandite during hydration. Prolonged curing and higher w/b ratios led to increased hydration.

The effect of fly ash and slag on hydration was followed via the ratio of actual to portlandite contents expected based on dilution [37] (CH_{act}/CH_{exp} in Table 3). By 28 days there was portlandite consumption, particularly for the slag-bearing systems. $CH_{actual}/CH_{expected}$ fell with increasing w/b, due to increased SCM hydration.

The CH content was greater in the PFA-containing samples at 3 days than in the equivalent GGBS blends, suggesting a lower extent of PFA hydration, consistent with the literature [41, 42]. But the change in CH_{act}/CH_{exp} was similar for the PFA and 30% GGBS samples

between 3 and 28 days, suggesting that the rate of portlandite consumption, and hence the approximate degree of hydration, over this time was similar for both SCMs.

Table 3: CH content, AFt contents following hydration for 72 hours and 28 days.

			CH/(100g binder)		CH_{act}/CH_{exp}	AFt/(100g binder)
	w/b	Time (d)	XRD	TGA	TGA	XRD
CEM I 52.5R	0.40	3	9.8	12.6	1.00	9.8
		28	13.2	15.3	1.00	12.9
30% PFA	0.40	3	7.7	11.2	1.27	7.3
		28	10.4	12.0	1.12	10.0
30% GGBS	0.40	3	7.6	9.3	1.05	7.8
		28	9.3	9.7	0.91	8.5
60% GGBS	0.40	3	4.3	5.5	1.09	5.6
		28	4.7	6.4	1.04	5.6
CEM I 52.5R	0.57	3	18.0	17.7	1.0	12.9
		28	22.6	21.3	1.0	11.9
30% PFA	0.57	3	11.4	14.2	1.14	10.0
		28	16.5	15.6	1.05	8.6
30% GGBS	0.57	3	9.8	12.8	1.03	9.3
		28	10.0	12.0	0.80	8.4
60% GGBS	0.57	3	3.6	7.3	1.03	5.1
		28	4.7	6.9	0.81	4.4

3.1.2 Phase assemblages

Table 3 presents the portlandite and AFt contents. Increased hydration led to higher portlandite contents over time for CEM I samples and at higher w/b ratios. The fly ash systems showed slight increases in portlandite content, but the more reactive slag led to portlandite consumption.

Cement replacement reduced AFt formation. At 3 days, AFt levels were higher at higher w/b, but this was reversed at 28 days. The poor crystallinity and susceptibility of the AFm phases to changes in composition and structure [43] prevented AFm contents quantification. XRD patterns are presented in the supplementary material (Figure S-1).

3.1.3 Microstructure

Analytical TEM was performed on selected samples at w/b ratio 0.57. The microstructure of the CEM I system was already well established by 72 hours (Figure S-2), agreeing with previous studies [49-51]. Homogenous, inner- (Ip) and outer-product (Op) regions with both coarse and fine fibrillar C-S-H were observed. AFt crystals occupied Op regions, evidenced by hexagonal, prism-shaped relicts (Figure S-2) arising from their decomposition under the electron beam [52].

Op regions in the 30% replacement systems (Figure 1) displayed both coarse and fine fibrillar C-S-H, appearing somewhat coarser than for the CEM I sample. Foil-like C-S-H confirmed reaction of both the PFA and GGBS [1, 24, 53, 54], confirmed by slight reaction rims on PFA particles (Figure 1). Ip regions, assumed to be predominantly alite, showed fine homogenous microstructures, and large irregular AFm plates were located in the relatively open Op regions. The low degree of reaction in the 60% GGBS system made it unsuitable for characterisation at 72 hours.

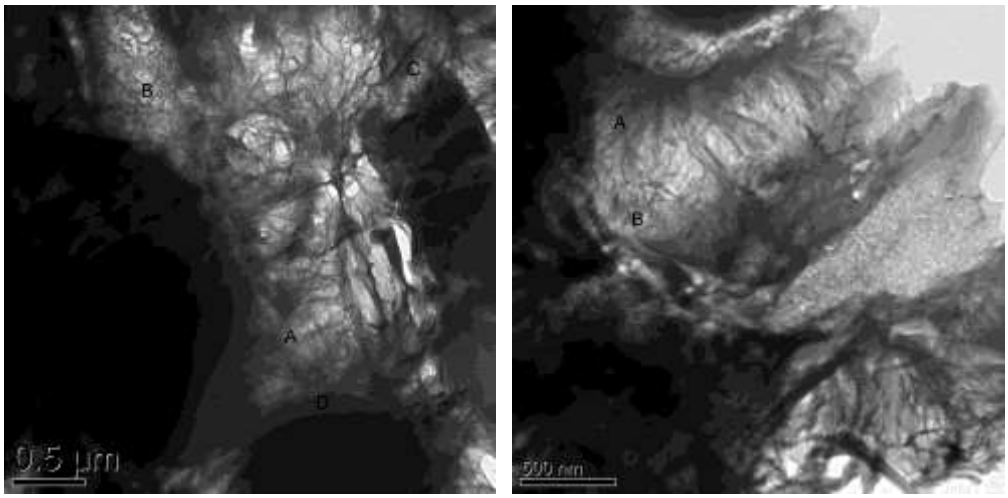

Figure 1. TEM micrographs of 72hr w/b 0.57 30% replacement specimens. a) 30% PFA sample showing fibrillar (A) and foil-like (B) Op regions, AFm (top right hand corner) (C) and slight reaction rims on PFA particles (D). b) 30% GGBS sample showing fibrillar (A) and foil-like (B) Op regions

By 28 days, the 30% PFA sample showed denser Op regions (Figure 2), with both fine fibrillar and foil-like morphologies. Ip C-S-H was more prevalent, but PFA reaction rims

remained small. Ben Haha et al. [41] measured levels of reaction of 2%, 21% and 35% for a 35% PFA sample at 1, 28 and 140 days respectively, highlighting the variability in fly ash reactivity. AFt relicts were observed in Op regions (Figure 3). Fully reacted cement grains display fine scale homogenous morphology.

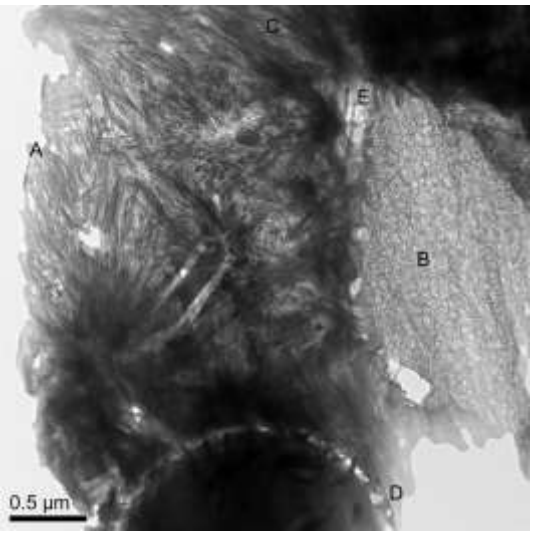

Figure 2. TEM micrographs of 30% PFA 0.57 (28d) sample showing fibrillar (A) and foil-like (B) Op regions, fine Ip regions (C), PFA reaction rims (D), and AFt relicts (E).

By 28 days, the higher degree of slag hydration was evident (Figure 3a). Op regions displayed a fine fibrillar morphology and foil-like C-S-H was more prevalent. The fine textured Ip C-S-H in Figure 3a was from slag hydration due to the presence of hydrotalcite laths and the presence of Mg in EDX data. Dense AFm plates were seen (Figure 3b). At 60% replacement (Figure 4) the Op C-S-H was crumpled foil like, consistent with the literature [24], and fine fibrillar C-S-H was observed only sparingly. Ip regions typically exhibited intermixing of C-S-H and hydrotalcite laths.

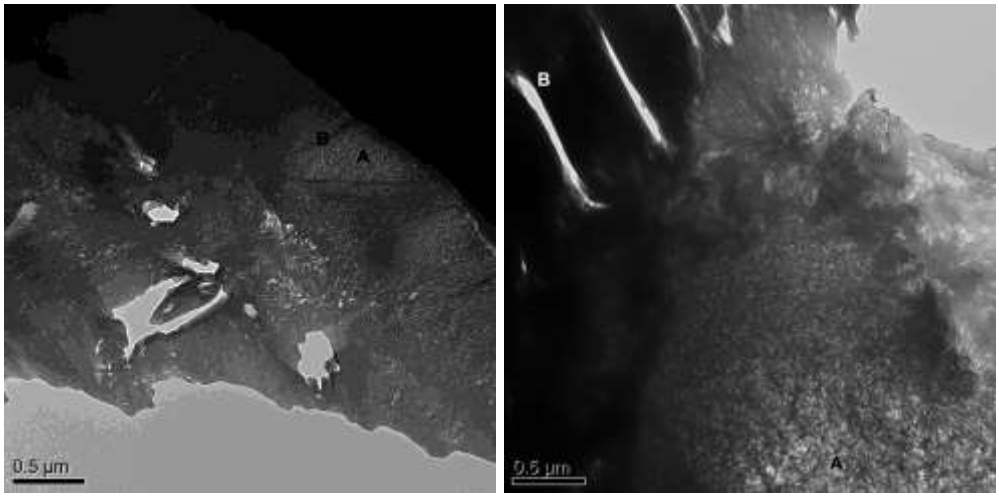

220

221 *Figure 3. TEM micrographs of 30% GGBS 0.57 (28d) – t_0 sample showing a) fine textured lp regions*

222 *(A) intermixed with laths of hydrotalcite (B), b) foil-like Op (A) and AFm plates (B).*

223

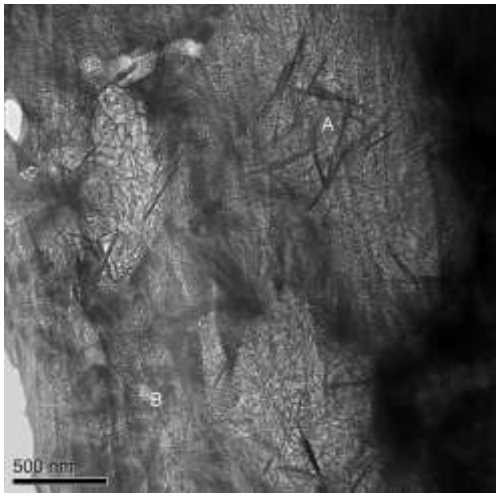

224

225 *Figure 4. TEM micrographs of 60% GGBS 0.57 (28d) sample showing fine textured lp regions*

226 *intermixed with hydrotalcite laths (A), foil-like and fine fibrillar (B) Op C-S-H.*

227

228 TEM-EDX data is displayed in Table 4 and Figure S-3. Mg/Si – Al/Si scatter plots for slag

229 containing systems (Figure S-4) confirmed lp regions to be mixtures of C-S-H and a Mg rich

230 hydrotalcite like phase [55].

231

232

Table 4. Mean Ca/Si and Al/Si ratios for selected w/b 0.57 samples analysed by TEM-EDX.

				Ca/Si		Al/Si		Mg/Al
			N	Mean	S.D.	Mean	S.D.	
CEM I	72h	Op	20	1.61	0.14	0.11	0.03	-
		Ip	25	1.72	0.21	0.07	-	-
		All	45	1.67	0.19	-	-	-
30% PFA	72h	Op	25	1.62	0.10	0.13	0.05	-
		Ip	19	1.53	0.08	0.11	0.02	-
		All	44	1.55	0.10	0.12	0.04	-
30% GGBS	72h	Op	50	1.48	0.18	0.16	0.07	-
		Ip	25	1.22	0.08	0.11*	-	2.78
		All	75	1.39	0.20	-	-	-
30% PFA	28d	Op	16	1.5	0.08	0.13	0.03	-
		Ip	27	1.49	0.14	0.13	0.01	-
		All	43	1.49	0.12	0.13	0.03	-
30% GGBS	28d	Op	-	-	-	-	-	-
		Ip	19	1.56	0.09	0.09*	-	2.72
		All	-	-	-	-	-	-
60% GGBS	28d	Op	32	1.27	0.07	0.15	0.01	-
		Ip	18	1.28	0.07	0.14*	-	2.5
		All	50	1.27	0.07	-	-	-

*Determined from regression analysis of Mg/Si – Al/Si plots at Mg/Si=0

Mg/Al ratio corresponds to Mg/Al ratio of hydrotalcite-like phase and was derived from regression analysis of Mg/Si – Al/Si plots

The average Ca/Si ratio for the neat system at 72 hours was 1.67, in good agreement with the literature [51]. Richardson and Groves [50] reported Ca/Si ratios of 1.69 and 1.65 for Op and Ip C-S-H in a week old Portland cement paste. The composite samples all showed lower Ca/Si and higher Al/Si ratios than the CEM I sample, confirming fly ash and slag reaction, as also seen in the ternary diagrams (Figure S-3). This was most marked for the 28d 60% slag sample, where the C-S-H had the lowest Ca/Si ratio (1.27) and highest Al/Si ratio (0.15 Op / 0.14 Ip). In the 30% replacement samples, the Ca/Si ratio was lower Al/Si ratio higher in the slag system reflecting the higher degree of slag hydration at 72h. Between 72 hours and 28 days the mean Ca/Si ratio for the PFA sample fell from 1.55 to 1.49, indicating that any PFA hydration between 72 hours and 28 days was relatively minor. See supplementary material Figure S-3 and accompanying text for further discussion.

The C-S-H was characterised quantitatively by deconvolution of ^{29}Si MAS NMR spectra so as to fit peaks corresponding to Q^0, Q^1, Q^2(1Al) and Q^2 species [55-58] (with further details in the supplementary material). The chemical shifts (δ) and relative fractions of the Q^1, Q^2(1Al) and Q^2 sites are presented in Table 5. Mean aluminosilicate chain lengths (MCL) and Al/Si ratios were determined using the equations presented in the supplementary material [1, 59].

Table 5. Results from deconvolution of single pulse ^{29}Si NMR spectra for each system at t_0. Al/Si ratios as determined by TEM-EDX for selected samples are included for comparison.

			Chemical shifts / δ (ppm)			Relative intensities (%)				Al/Si		
	w/b	Time	Q^1	Q^2(1Al)	Q^2	Q^1	Q^2(1Al)	Q^2	MCL	NMR	TEM [s.d.]	
											Ip	Op
CEM I	0.40	72h	-78.62	-81.67	-84.42	69	15	16	3.1	0.07	-	-
30% PFA	0.40	72h	-78.7	-81.85	-84.46	70	15	16	3.1	0.07	-	-
30% GGBS	0.40	72h	-78.68	-81.54	-84.46	60	21	19	3.7	0.10	-	-
60% GGBS	0.40	72h	-78.82	-81.44	-84.26	59	17	24	3.7	0.09	-	-
CEM I	0.40	28d	-78.7	-81.72	-84.54	64	16	20	3.4	0.08	-	-
30% PFA	0.40	28d	-78.83	-81.72	-84.63	59	17	25	3.7	0.08	-	-
30% GGBS	0.40	28d	-78.71	-81.4	-84.29	53	21	26	4.2	0.11	-	-
60% GGBS	0.40	28d	-78.84	-80.94	-84.24	39	28	33	5.9	0.14	-	-
CEM I	0.57	72h	-78.75	-81.80	-84.27	74	14	12	2.9	0.07	0.07	0.11 [0.03]
30% PFA	0.57	72h	-78.56	-81.44	-84.11	59	19	22	3.7	0.10	0.11 [0.02]	0.13 [0.05]
30% GGBS	0.57	72h	-78.84	-81.68	-84.68	61	22	18	3.7	0.11	0.11	0.16 [0.07]
60% GGBS	0.57	72h	-79.11	-81.22	-84.29	38	27	35	6.0	0.13	-	-
CEM I	0.57	28d	-78.72	-81.57	-84.46	64	14	21	3.3	0.07	-	-
30% PFA	0.57	28d	-78.58	-81.22	-84.24	48	21	31	4.5	0.11	0.13 [0.01]	0.13 [0.03]
30% GGBS	0.57	28d	-78.77	-81.32	-84.45	46	22	32	4.8	0.11	0.09	-
60% GGBS	0.57	28d	-78.69	-80.83	-84.05	35	32	33	6.6	0.16	0.14	0.15 [0.01]

Systems with w/b ratio 0.40 cured for 72 hours displayed similar relative fractions of Q^1, Q^2(1Al) and Q^2 sites, indicating similar levels of clinker hydration and C-S-H composition, plus a low degree of PFA and GGBS reaction at this age. However, slight increases in MCL and Al/Si ratios for the slag systems compared with the CEMI and fly ash samples indicated slight slag hydration by 72h, consistent with TGA data. Changes in C-S-H composition were more evident at w/b ratio 0.57. For the 30% slag system composition, MCL and Al/Si ratios were similar. However, increased polymerisation (transition from Q^1 to Q^2) and higher Al/Si ratios were observed for the 30% PFA and 60% slag samples. This supports the TGA data showing increased hydration at higher water contents.

At both w/b ratios, hydration had progressed, resulting in increased MCL and Al/Si ratios as levels of substitution increased. These changes were more pronounced in the w/b 0.57 samples. The MCL also increased for the CEM I systems, but with no change in Al/Si ratio.

3.2 Early age carbonation behaviour (t_0-7 days)

3.2.1 Changes in the phase assemblage

3.2.1.1 Thermal Analysis

Samples stored in a CO_2–free atmosphere for up to 60 days (Figures S-5 and S-6) showed no additional hydration during sample conditioning at RH 72.6%, agreeing with previous work reporting no significant hydration below 80% RH [21]. Therefore, any changes observed upon exposure to ambient CO_2 were a direct result of carbonation.

Figure 5 displays the $Ca(OH)_2$ and $CaCO_3$ contents derived from TGA data. Exposure to CO_2 led to an increase in total carbonate content. However, the carbonate content increased significantly in the 72 hour cured samples (Figure 5(a)) upon the complete, or almost complete, consumption of portlandite. This was observed for all of the systems, but at earlier exposure times with increasing replacement levels: between 4 – 7 days for the neat system, 2 – 4 days for the 30% replacement systems and between 1 – 2 days for the 60% GGBS system. The quantity of $CaCO_3$ produced was also greatest in the composite materials.

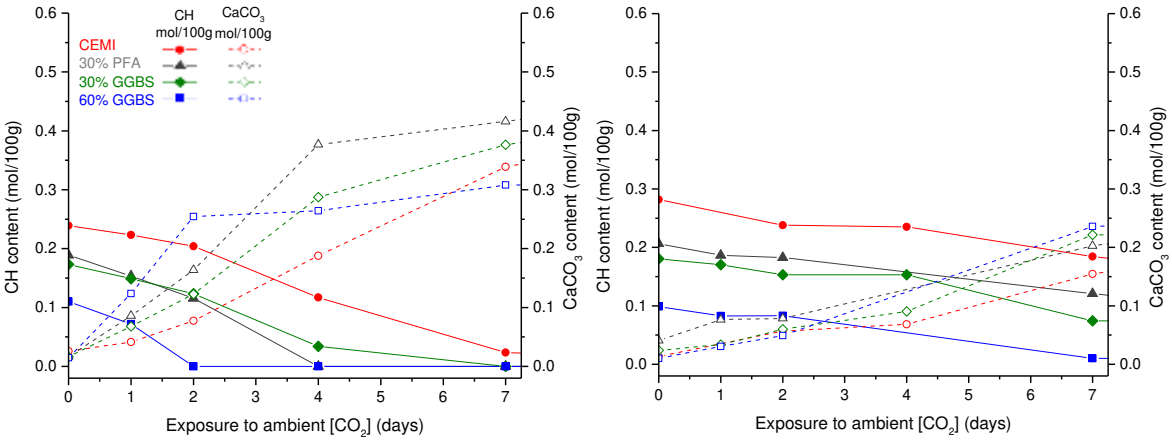

Figure 5. CH and $CaCO_3$ contents determined from TGA data for 72 hour cured (a) and 28 day cured (b) w/c = 0.57 systems following exposure to ambient [CO_2] for up to 7 days.

The presence of CH acts as a buffer against carbonation of other phases. Consumption of CH led to loss of buffering capacity and carbonation progressed much more rapidly. Continued carbonation following portlandite consumption indicated that carbonation of the other phases had become significant. This is reflected in Table 6, which displays the consumption of portlandite and corresponding production of $CaCO_3$ between 0 (t_0) and up to

295 7 days exposure to CO_2. The quantity of $CaCO_3$ produced from hydrate phases other than
296 portlandite is shown in the last column.

297 The extent of carbonation was affected by both replacement material and level. At equivalent
298 levels of replacement, there was more, and faster, carbonation of the PFA blend; reflecting
299 PFA's slower reaction rate. The adverse effects of slower hydration on carbonation
300 resistance are expected to be magnified with shorter curing length and increasing
301 replacement. This is reflected in the much faster initial carbonation rate of the 3 day cured
302 60% GGBS system. As carbonation progressed, however, a plateau was reached (from 2
303 days onwards) by which time all the hydrate phases available for carbonation had reacted.

304

305 *Table 6. Consumption of CH versus production of $CaCO_3$ calculated from TGA data between t_0 – 7*
306 *days for 72 hour cured systems and at 7 days for 28 day cured systems (w/c 0.57).*

	$Ca(OH)_2$ consumed (mol/100g)	$CaCO_3$ produced (mol/100g)	$CaCO_3$ produced from other hydrates (mol/100g)
CEM I			
1 day	0.02	0.02	0.00
2 days	0.04	0.05	0.01
4 days	0.12	0.16	0.04
7 days	0.22	0.31	0.09
(28d) 7 days	0.10	0.14	0.04
30% PFA			
1 day	0.04	0.07	0.03
2 days	0.07	0.15	0.08
4 days	0.19	0.36	0.17
7 days	0.19	0.40	0.21
(28d) 7 days	0.09	0.16	0.08
30% GGBS			
1 day	0.02	0.05	0.03
2 days	0.05	0.11	0.06
4 days	0.14	0.27	0.13
7 days	0.17	0.36	0.19
(28d) 7 days	0.11	0.20	0.09
60% GGBS			
1 day	0.03	0.11	0.08
2 days	0.10	0.24	0.14
4 days	0.10	0.25	0.15
7 days	0.10	0.29	0.19
(28d) 7 days	0.08	0.23	0.14

307

308 The TGA data highlights the adverse effects of improper curing on blended cements, where
309 slower rates of hydration and curing lengths of only a few days, produced materials with
310 underdeveloped, open microstructures, through which CO_2 could diffuse readily. This poor
311 carbonation resistance was further exacerbated by lower initial portlandite levels, which
312 decreased further with increasing substitution.

313 Similar behaviour was reported by Thiery *et al*. [19] on samples cured for 8 months then
314 carbonated in a ~50% CO_2 atmosphere. Carbonation of portlandite was initially much faster
315 than that of C-S-H. But the formation of $CaCO_3$ microcrystals on the portlandite crystal
316 surfaces inhibited further reaction, allowing decalcification of C-S-H to then proceed more
317 vigorously. Groves *et al*. [17] discussed the carbonation of C_3S pastes in both air and pure
318 CO_2. Again, the initial rate of portlandite carbonation was much faster, with the rate dropping
319 upon carbonation of the C-S-H. In pure CO_2 atmospheres this was due to microcrystalline
320 carbonate crystals coating the portlandite crystals. But there was no evidence for this with
321 samples exposed to air.

322 For the samples cured for 28 days, Figure 6(b), prolonged exposure to CO_2 led to increased
323 carbonate production, but far less than was observed in the immature systems. Portlandite
324 was still present in appreciable quantities following 7 days' exposure to CO_2 in the CEM I
325 and 30% replacement systems, but it had been almost entirely consumed in the 60% slag
326 sample. The reduced carbonation resistance of the 60% GGBS systems was again
327 attributed to a combination of its much lower initial portlandite content and degree of
328 reaction. Borges *et al*. [60] related the mechanism of slag cement carbonation to the
329 available portlandite content prior to exposure to CO_2.

330 As with the samples cured for 3 days, following 28 days' curing there was slight carbonation
331 of the other hydrates in the presence of portlandite (Table 6). The extent of this was
332 significantly less than for the 3 day samples. Despite this, there was still a similar
333 relationship between the extent of carbonation and replacement level, with carbonate
334 formation increasing with substitution level. Since substitution results in lower initial

335 portlandite contents, the proportion of carbonate formed from carbonation of phases other
336 than portlandite increased with increasing substitution.

337 Carbonation of non-portlandite phases will affect C-S-H, AFt and AFm phases. However it is
338 not clear how the calcium aluminate phases react, or to what extent they react, in the
339 presence of portlandite upon exposure to ambient air. Early age carbonation of AFt and AFm
340 phases has been observed but under accelerated conditions [61, 62]. Meanwhile, Chen *et*
341 *al*. [22] observed that C-S-H with lower Ca/Si, such as formed in blended systems, is more
342 vulnerable to abstraction of Ca.

343 In addition to revealing the extent of carbonation, thermal analysis revealed a change in
344 carbonate speciation. Progressive carbonation led to carbonate decomposition at lower
345 temperatures (Table 7) for some of the systems. This coincided with both the loss of
346 portlandite and the significant increase in carbonate content previously observed. This
347 strongly indicated decalcification of C-S-H produced poorly crystalline, metastable calcium
348 carbonate, in line with the three calcium carbonate decomposition modes proposed by
349 Thiery [19]. Shi *et al*. [63] reported decomposition of $CaCO_3$ beginning at lower temperatures
350 for heavily carbonated surface regions of mortar samples, observing decomposition
351 temperatures as low as 250°C for metakaolin and limestone containing materials.

352

353 *Table 7. Temperature at which mass loss due to $CaCO_3$ decomposition begins (w/b = 0.57). (note that*
354 *data for 28 day 30% PFA exposed for 4 days is missing)*

	72 hours					28 days				
	Length of exposure to ambient CO_2 (days)					Length of exposure to ambient CO_2 (days)				
	0	1	2	4	7	0	1	2	4	7
CEM I	550	560	550	530	**455**	560	580	550	550	540
30% PFA	550	540	530	**410**	400	550	540	550	-	550
30% GGBS	580	540	530	**450**	450	580	560	560	540	540
60% GGBS	550	520	**310**	350	300	580	550	540	530	**480**

355

356 The formation of thermally-unstable calcium carbonate via carbonation of C-S-H was
357 confirmed by carbonation of a portlandite-free C-S-H sample (Figure S-7). TG-FTIR data

(Figure S-8) further confirmed that the mass loss was almost entirely a result of the presence of carbonate species.

DTA data (not shown) revealed the presence of AFm in all systems at t_0. Carbonation led to the diminishment and disappearance of peaks ascribed to AFm, indicating the early-age carbonation of AFm species. Prior to their disappearance, signals due to AFm phases shifted to lower decomposition temperatures for the 60% slag system between 0 – 4 days, indicating transformation of the AFm species [43] before complete decalcification. There was subsequently a distinct peak at ~130°C in the same system at 7 days due to gypsum, indicating carbonation of AFt [61, 66]. Similar behaviour was seen for 28 day samples. AFm peaks diminished with carbonation, shifting to lower temperatures as carbonates displaced sulphates [43]. Complete dissociation of AFm, however did not occur.

As for the w/b 0.57 samples, both 72 hour and 28 day cured specimens with w/b 0.4 showed reduced carbonation with increasing curing length and increasing initial portlandite content. In all cases carbonation was reduced at lower w/b, (Figure 6, Table 8). Despite the lower water content resulting in lower initial portlandite contents, this phase was still present following 7 days' exposure in the neat and 30% replacement systems cured for 72 hours. This contrasts the complete consumption of portlandite in the equivalent w/b 0.57 samples. The 60% slag system showed almost complete portlandite consumption after curing for 72 hours, indicating poor resistance to carbonation following short curing periods. TGA (Figure S-8) further established acceleration of carbonation upon consumption of CH, accompanied by a significant decrease in carbonate decomposition temperature. The beginning of a more aggressive carbonation mechanism is associated with vigorous decalcification and dealumination of the C-S-H gel (TEM-EDX data – Section 3.2.2.1) and decalcification of the remaining Ca bearing hydrate phases.

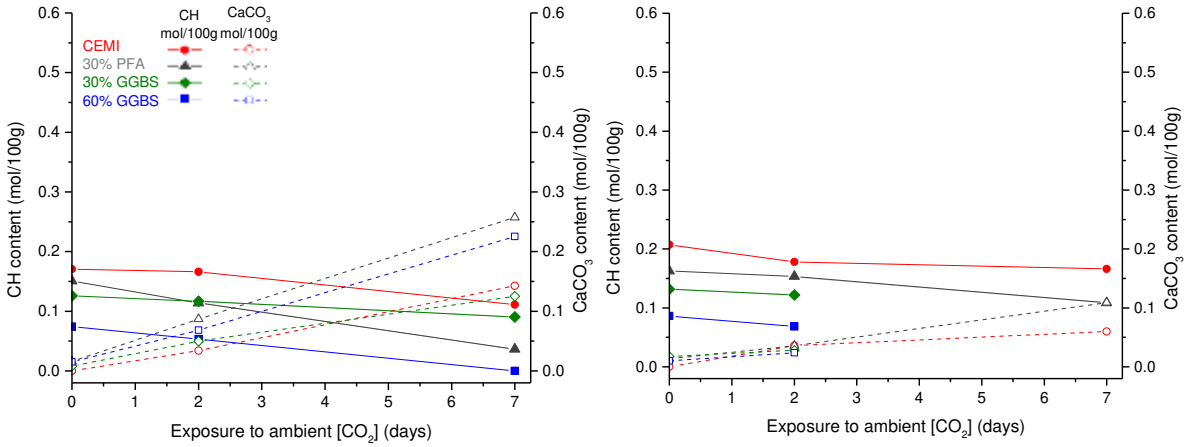

383

384 *Figure 6. CH and $CaCO_3$ contents determined from TGA data for 72 hour cured (a) and 28 day cured*

385 *(b) (0.40 w/b) systems following exposure to ambient [CO_2] for up to 7 days.*

386

387 *Table 8. Consumption of CH versus production of $CaCO_3$ calculated from TGA data following 7 days*

388 *exposure to ambient [CO_2] for 72 hr and 28 day cured systems (w/c 0.40). (*measurement taken at 2*

389 *days).*

	72 hours			28 days		
	$Ca(OH)_2$ consumed (mol/100g)	$CaCO_3$ produced (mol/100g)	$CaCO_3$ produced from other hydrates (mol/100g)	$Ca(OH)_2$ consumed (mol/100g)	$CaCO_3$ produced (mol/100g)	$CaCO_3$ produced from other hydrates (mol/100g)
CEM I	0.06	0.14	0.06	0.04	0.06	0.02
30% PFA	0.11	0.24	0.13	0.05	0.10	0.04
30% GGBS	0.04	0.16	0.12	0.01*	0.01*	0.00*
60% GGBS	0.07	0.21	0.14	0.02*	0.02*	0.00*

390

391 3.2.1.2 XRD

392 XRD revealed mineralogical changes upon carbonation of samples cured for 72 hours

393 (Figure 7) and 28 days (Figure 8). Carbonation of the 72h systems led to portlandite

394 consumption and predominantly calcite formation. AFm reflections were weak and poorly

395 resolved, but peaks diminished and shifted, particularly after almost portlandite complete

396 depletion. AFt contents remained relatively constant until portlandite had almost entirely

397 reacted, whereupon they diminished notably, consistent with DTA data.

398

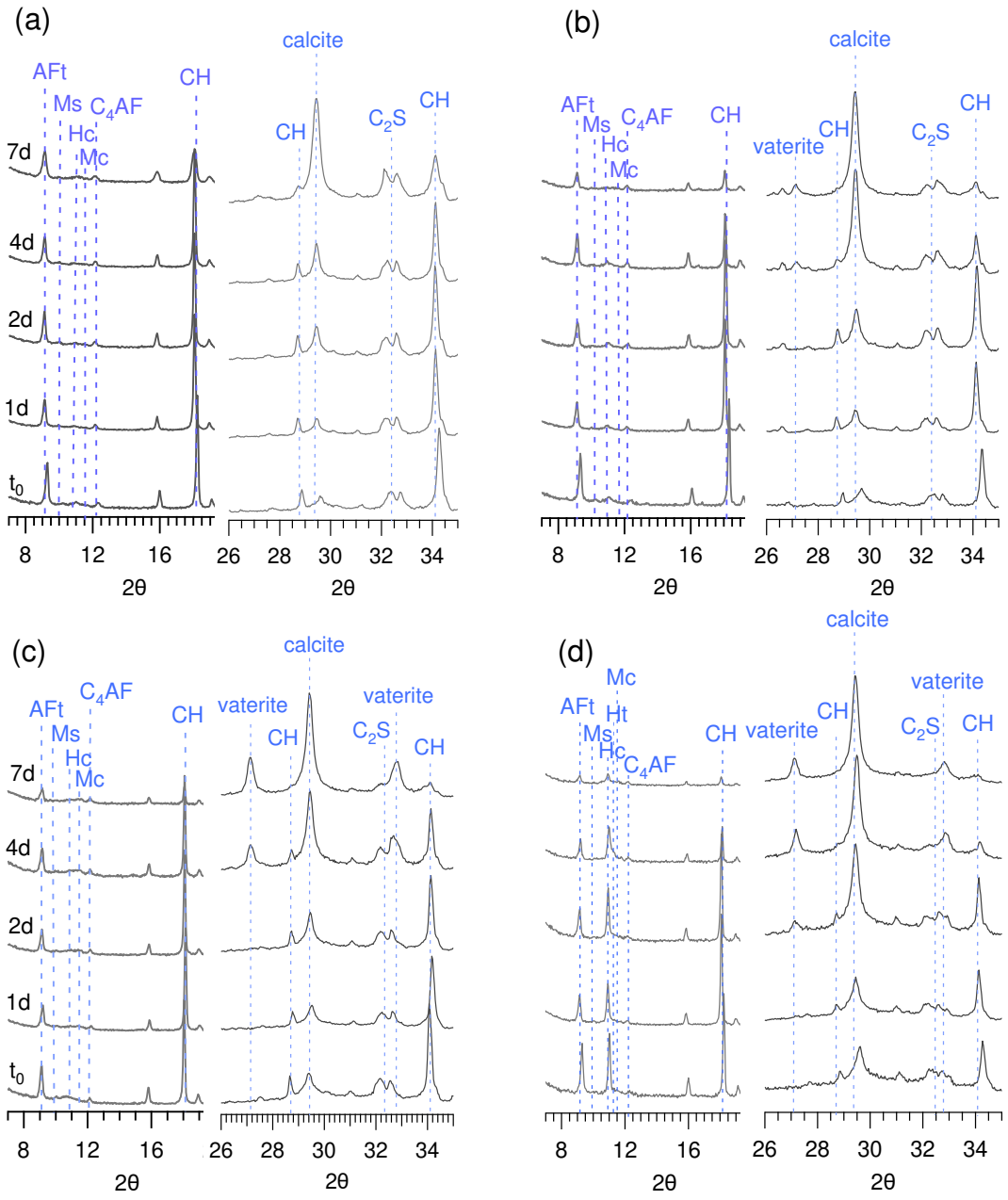

Figure 7. XRD patterns showing mineralogical changes upon exposure to ambient [CO_2] (t_0 – 7 days) for 0.57 (w/b) 72 hour cured samples (a) CEMI, (b) 30% PFA, (c) 30% GGBS, (d) 60% GGBS (AFt – ettringite, Ms – monosulfoaluminate, Hc – hemicarboaluminate, Mc – monocarboaluminate, Ht – hydrotalcite).

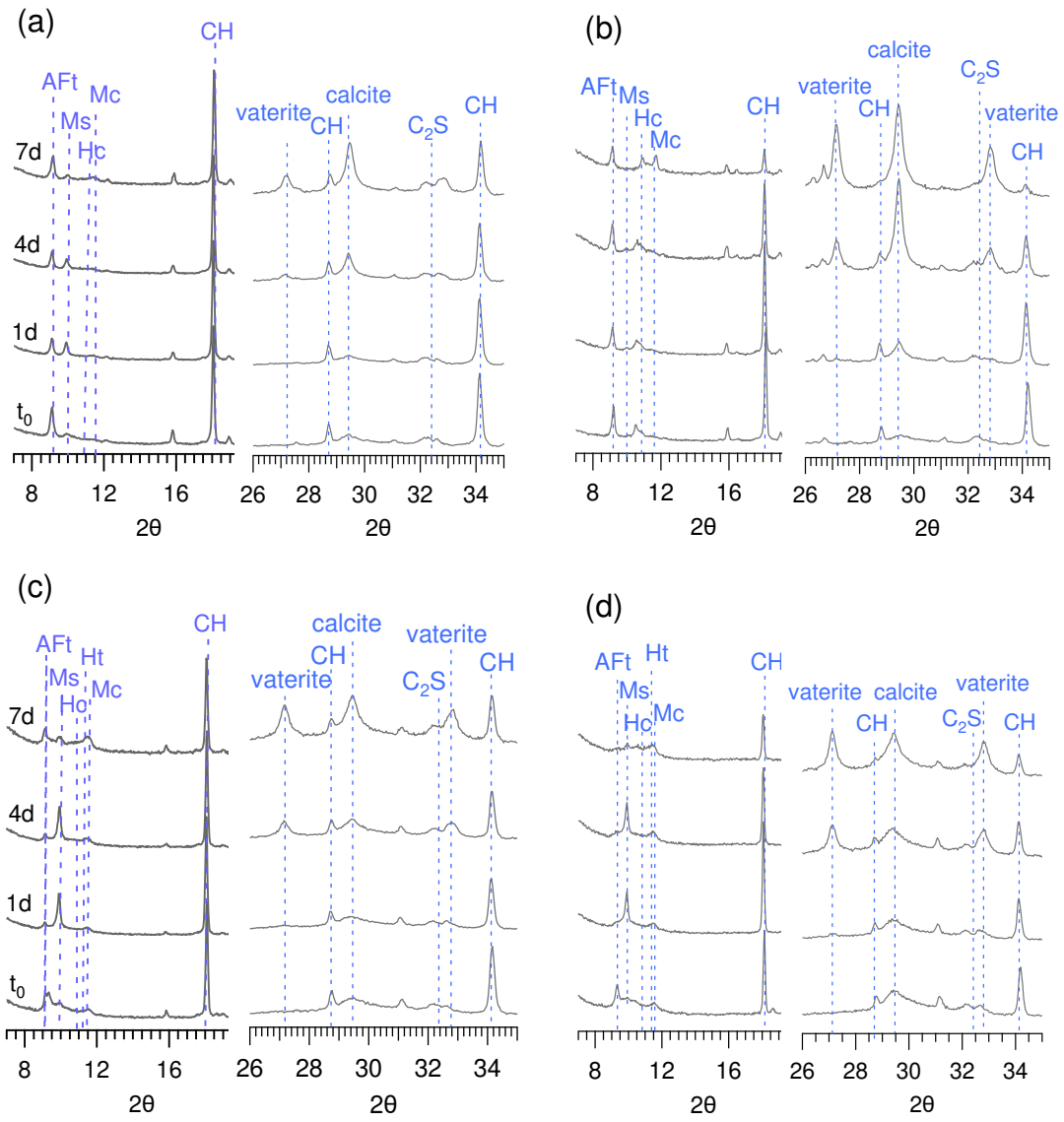

406

407

408 *Figure 8. XRD patterns showing mineralogical changes upon exposure to ambient [CO_2] (t_0 – 7 days)*

409 *for 0.57 (w/b) 28 day cured samples (a) CEMI, (b) 30% PFA, (c) 30% GGBS, (d) 60% GGBS.*

410

411 As shown by thermal analysis, carbonation was reduced in the samples cured for 28 days,

412 and portlandite remained up to 7 days' exposure (Figure 8). Peaks due to AFm phases were

413 sharper and conversion of AFt to monosulfoaluminate or hemicarboaluminate between t_0

414 and 1 day occurred in nearly all systems. Subsequently, there was conversion of mono-

415 sulfoaluminate to hemi- and monocarboaluminate, as inferred from DTA plots. This was

416 most clearly seen in the fly ash sample (Figure 8(b)). Beyond 1 day, AFt, contents remained

417 relatively consistent, further supporting the opinion that while portlandite is available,
418 decomposition of this phase remains relatively low.

419 In agreement with thermal analysis data, XRD revealed differences in the carbonate
420 polymorphs formed between the two curing conditions, particularly for the composite
421 materials. Short curing periods resulted in the formation predominantly of calcite, with traces
422 of vaterite from 4 days' exposure in the fly ash and slag samples. Prolonged curing,
423 however, led to increased vaterite formation, particularly in the slag blends.

424 The formation of calcite and vaterite in carbonated cements is not uncommon. Groves *et al*.
425 [17] observed both polymorphs in C_3S pastes carbonated in air and pure CO_2, with calcite
426 predominant at the surface and both polymorphs present sub-surface. Similarly, both calcite
427 and vaterite were formed upon carbonation of a C_3S – silica fume blend [20], with vaterite
428 almost entirely disappearing following carbonation for 8 days in pure CO_2. Fluctuations in
429 relative levels of vaterite and calcite after prolonged carbonation were also observed for 20
430 year old slag-bearing pastes exposed to natural and accelerated CO_2 conditions [67]. Lower
431 slag loadings yielded vaterite earlier, while at later ages higher loadings resulted in reduced
432 vaterite contents, attributed to transformation to the more stable calcite. Thiery *et al*. [19] and
433 Villain *et al*. [29] both showed vaterite to be the product of C-S-H decalcification. Similarly,
434 Sauman [68] observed C-S-H carbonation to initially form vaterite, later transforming to
435 calcite. Dubina *et al*. [70] meanwhile, showed that carbonate speciation was affected by the
436 relative humidity of the carbonating environment. An amorphous carbonate formed when
437 CaO was exposed to air at 20% RH, all three crystalline polymorphs co-existed between 20
438 – 60% RH and calcite was dominant as the humidity level increased further (60-80%).

439 Aragonite was almost entirely absent from the carbonated systems studied here and an
440 inverse relationship between the formation of vaterite and the initial CH content appears to
441 exist. The initial Ca/Si ratio can define the carbonate polymorph formed upon carbonation of
442 synthetic C-S-H [71], with aragonite forming in the presence of free silica and vaterite
443 forming when C/S > 0.67. Thus the absence of aragonite in this study is not unsurprising.

While Black et al. did not observe calcite formation, this is likely due to the carbonation conditions, where the C-S-H samples were dried before carbonation in ambient air. This would likely keep the relative humidity low enough to minimise calcite formation.

At the lower w/b ratio (0.40) following 72 hours' curing, the neat and 30% replacement systems showed only slight changes in hydrate assemblages upon carbonation. AFt reflections remained unchanged and portlandite levels decreased slightly (Figure 9). AFm reflections were poorly resolved but still present following exposure for 7 days.

There was complete portlandite consumption in the 60% slag system, with considerable calcite formation. Both AFt and AFm were consumed, with only small amounts still present at 7 days. Calcite was predominant in all the systems, however small reflections for vaterite were also observed for the 60% GGBS sample. Following 28 days' curing, the CEMI and 30% PFA sample showed almost no change in the crystalline phase assemblage except for small reflections due to calcite following exposure to CO_2.

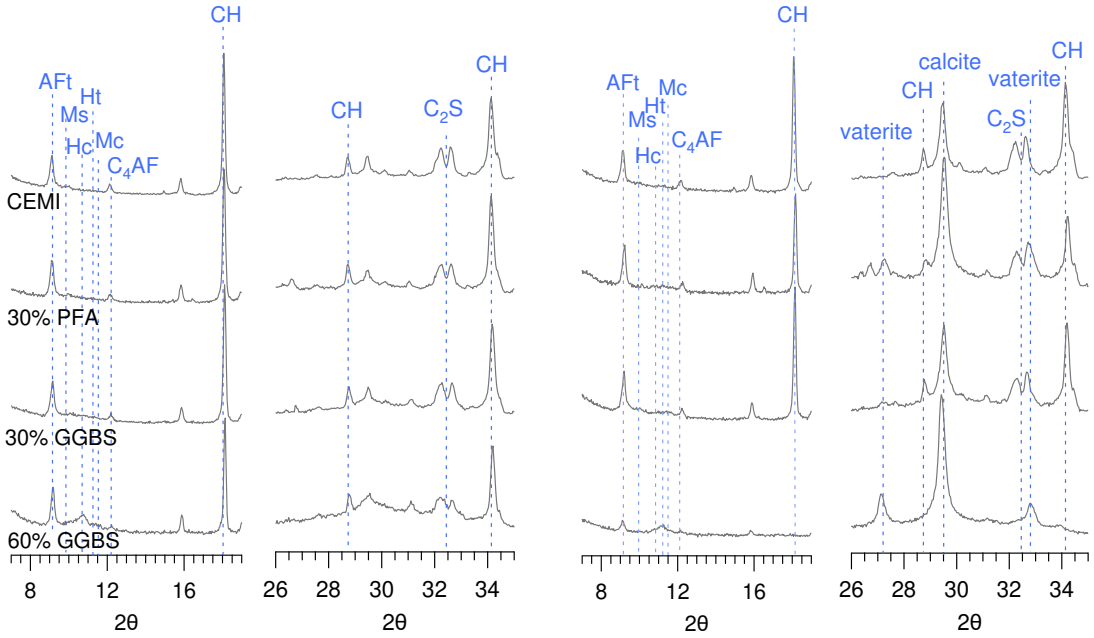

Figure 9. XRD patterns between 7 – 19° 2θ and 26 – 35° 2θ showing the crystalline phase assemblage of 0.40 (w/b) 72 hour cured systems at (a) t_0 and (b) following 7 days' exposure to ambient CO_2.

462 3.2.1.3 ATR-FTIR

463 Figure 10 displays the ATR-FTIR spectra from the CEM I and 30% PFA samples exposed to
464 ambient CO_2 for up to 7 days. There was growth in the carbonate band between 1400 –
465 1500cm^{-1} [72-74] upon exposure, with a sizeable jump between 4 and 7 days and 2 and 4
466 days for the neat and PFA samples respectively. This is explained by examining the bands
467 assigned to silicates (~1000 cm^{-1}) and portlandite (3643cm^{-1} [72]). Portlandite was
468 consumed during carbonation, with no changes in the silicate bands while portlandite was
469 present. Once portlandite was consumed, there was a shift in the silicate band to higher
470 wavenumbers, attributed to C-S-H decalcification [73]. Thus, loss of buffering capacity upon
471 portlandite consumption allowed carbonation to progress much more rapidly. For this
472 reason, the less mature samples, or those containing less clinker, showed C-S-H
473 decalcification at earlier ages, consistent with STA and XRD data discussed previously.

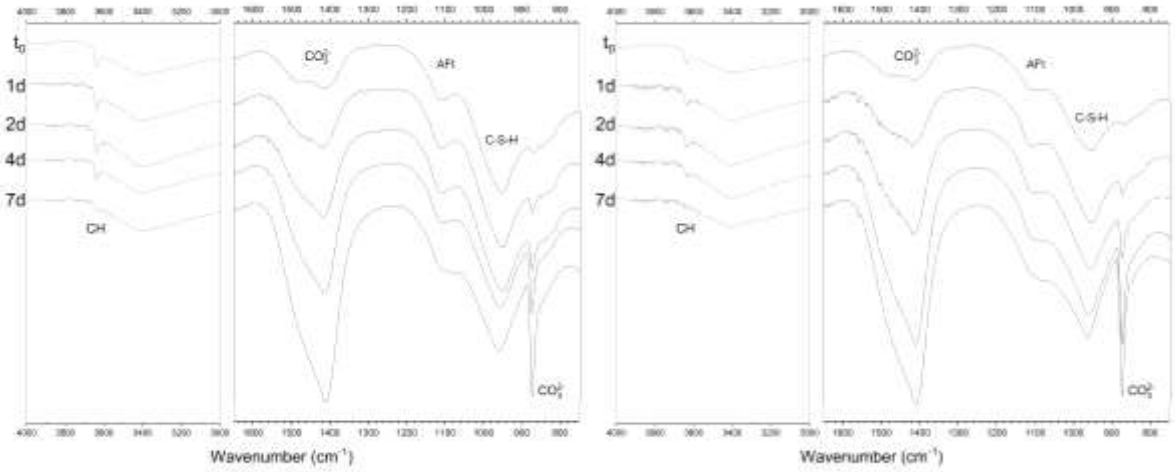

474

475 *Figure 10. ATR-FTIR spectra for 0.57 - 72hr CEMI (a) and 30% PFA (b) blends showing bands*
476 *ascribed to portlandite (~3640 cm^{-1}), carbonate (1400–1500cm^{-1}), AFt (~1120cm^{-1}), silicate (~950-*
477 *1000cm^{-1}) and calcite (~870cm^{-1}).*

478

479 The ATR-FTIR spectra also inferred changes in carbonate speciation with time, with strong,
480 broad asymmetrical stretching bands (ν_3) between 1400 – 1500cm^{-1} and a sharper out of
481 plane bending band (ν_2) between ~850 – 880cm^{-1} [73, 74]. Calcite and vaterite both exhibit

similar ν_2 bands, at ~877cm^{-1} [74], while aragonite exhibits a band at ~854cm^{-1}, as does amorphous calcium carbonate (~864cm^{-1}). For amorphous carbonate the ν_3 band is split, showing two maxima [74], while crystalline modifications typically show sharper bands. While XRD showed calcite to be the predominant crystalline polymorph formed in the 72 hour cured samples, ATR-FTIR spectra after short periods of carbonation showed a broader, split ν_3 band, suggesting the initial formation of an amorphous product, as reported elsewhere [70, 71]. Further carbonation then led to the appearance and growth of a sharper, asymmetrical ν_3 band, accompanied by an increasingly intense band at 872cm^{-1}, supporting the XRD identification of calcite. Nevertheless, lower TGA decomposition temperatures following consumption of portlandite suggested that a poorly crystalline carbonate had also been formed, but it was not possible to deconvolute FTIR signals from both species.

Whilst only visible as a shoulder, the most intense AFt band, a strong asymmetrical stretching band at ~1120cm^{-1} [75, 76], remained unchanged during early age exposure, corroborating XRD results.

In the systems cured for 28 days, bands due to vaterite were prominent, particularly for the slag containing cements. The broad ν_3 bands due to amorphous carbonate were gradually replaced by sharper bands due to crystalline carbonates. Calcite was identified in the 30% system, while a peak shape more typical of vaterite [74] was observed for the 60% sample (Figure 11). Unlike upon carbonation of the 72 hour old samples, there was no complete consumption of portlandite and thus no shift in frequency of the silicate bands, indicating no significant C-S-H decalcification.

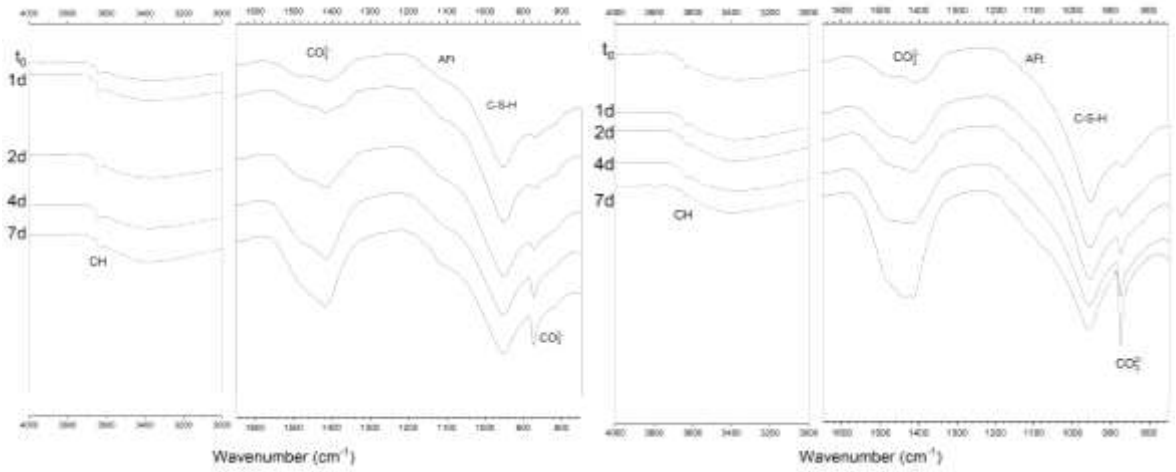

503

504 *Figure 11. ATR-FTIR spectra for 0.57 - 28 day 30% (a) and 60% GGBS (b) blends showing bands*

505 *ascribed to portlandite (~3640 cm^{-1}), carbonate ν_3 (1400–1500cm^{-1}) and ν_2, (~870cm^{-1}), silicate (~950-*

506 *1000cm^{-1}) and AFt (~1120cm^{-1}).*

507

508 3.2.2 Changes in the microstructure

509 3.2.2.1 TEM-EDX

510 TEM-EDX data are displayed in Figure 12 and Table 9 for two samples: 30% GGBS, w/b

511 0.57, cured 72 hours and carbonated for 4 days, 60% GGBS, w/b 0.57, cured for 28 days

512 and carbonated for 2 days. Carbonation led to decalcification, shown by the lower Ca/Si

513 ratios for both Ip and Op. Dealumination of Ip and Op regions was also observed for the 30%

514 slag system. In the 60% slag system, slight dealumination of Ip regions was observed but

515 the Al/Si ratio of the Op product C-S-H remained unchanged. Mg/Si–Al/Si plots revealed no

516 change in the Mg/Al ratio of the hydrotalcite-like phase in slag Ip regions (Figure S-4 (b)). Ip

517 analyses collected for the 30% GGBS sample (Figure S-4 (a)) suggested the presence of

518 only one phase (C-S-H) in the carbonated material.

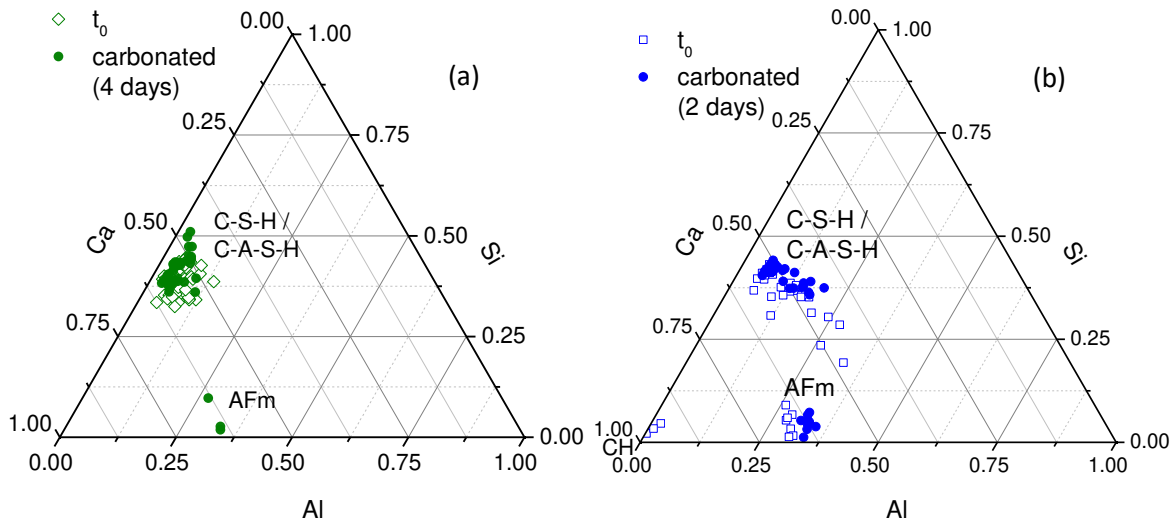

Figure 12. Ca-Al-Si ternary diagrams for (a) 30% GGBS 0.57 (72hr) and (b) 60% GGBS 0.57 (28d) systems showing EDX data collected for t_0 and carbonated samples. Values are plotted as atomic percentages normalised to 100%.

Table 9. Mean Ca/Si and Al/Si ratios for selected samples analysed by TEM-EDX.

			Ca/Si		Al/Si		Mg/Al
		N	Mean	S.D.	Mean	S.D.	
30% GGBS, 0.57, 72h, 4 days in ambient CO_2	Op	13	1.41	0.14	0.09	0.02	-
	Ip	16	1.16	0.13	0.10	0.03	-
	All	29	1.27	0.18	0.09	0.03	-
60% GGBS, 0.57, 72h, 2 days in ambient CO_2	Op	19	1.23	0.04	0.15	0.01	-
	Ip	18	1.21	0.07	0.125*	-	2.5
	All	37	1.22	0.06	-	-	-

* Determined form regression analysis of Mg/Si – Al/Si plots at Mg/Si=0

Mg/Al ratio corresponds to Mg/Al ratio of hydrotalcite-like phase and was derived from regression analysis of Mg/Si – Al/Si plots

Thermal analysis has previously shown carbonate formation via carbonation of phases other than portlandite. TEM-EDX data confirmed that calcium was supplied by the C-S-H phase irrespective of the presence of portlandite (Figure S-3). ATR-FTIR suggested C-S-H decalcification in the samples cured for 72 hours, but not in the more mature 28 day samples. TEM-EDX however showed C-S-H decalcification in both systems, with similar degrees of decalcification in both samples upon exposure to CO_2. However, Al abstraction was more pronounced in the 30% GGBS sample, which had been exhausted of portlandite.

Decalcification of C-S-H in ambient CO_2 atmospheres is a relatively slow process. Groves *et al*. [17] reported a decrease in the Ca/Si ratio of a 9 month cured C_3S paste exposed to ambient CO_2 for 2 months from 1.7 in the fresh sample to 1.02 after carbonation. Castellote *et al*. [27] reported a decrease from 1.87 to 1.23 for a 28 day cured Portland cement paste exposed to ambient CO_2 for 8 months.

Here, decalcification was much faster, with significant reductions in Ca/Si following only 2 and 4 days' exposure. Li [67] looked at carbonation of 25 year old 25% slag samples, measuring a Ca/Si ratio of 1.45-1.55 after carbonation (ambient [CO_2]) for 15 days, falling to 1.1-1.35 after carbonation for 60 days. Early age carbonation (15 days) for 75% and 90% GGBS systems resulted in Ca/Si ratios of ~1.15-1.2 and ~0.75 respectively. However, they observed that dealumination was more extensive than decalcification, with all aluminium abstracted from a carbonated 25% slag sample in which considerable quantities of calcium were still present. The EDX data collected here for the 30% slag system suggested similar behaviour, with more extensive removal of aluminium than calcium.

Carbonation occurred without significant changes in the morphology, (Figures 13 and 14). For both the 72 hour cured (30% slag) and 28 day cured (60% slag) samples, AFm plates remained solid and dense and Ip regions retained the fine scale homogenous morphology observed in the non-exposed materials. Slight coarsening of foil-like Op regions in the 72 hour cured sample was sometimes observed (Figure 13 (a)), but generally the morphology remained unaltered, in agreement with previous studies [18, 20, 67]. Calcite microcrystals were observed in Op regions only (highlighted with arrows in Figure 13 (b)). There was little evidence of carbonation in the 28 day cured 60% GGBS system exposed for 2 days. Op C-S-H generally appeared free from microcrystalline $CaCO_3$, although some areas yielded SAED patterns indicative of partially crystalline phases. Conversely, Figure 14 (a) shows carbonate microcrystals formed on Op C-S-H fibrils, but SAED patterns from these areas were diffuse rings indicating an amorphous phase. Loss of Ca from Ip C-S-H (determined by EDX analysis) did not affect its fine-scale morphology, which suggests Ip shrinkage upon

carbonation. Groves *et al*. [20] proposed this to be the cause of carbonation shrinkage; the Ca^{2+} cations migrating from Ip to Op regions in order to maintain equilibrium due to a concentration gradient.

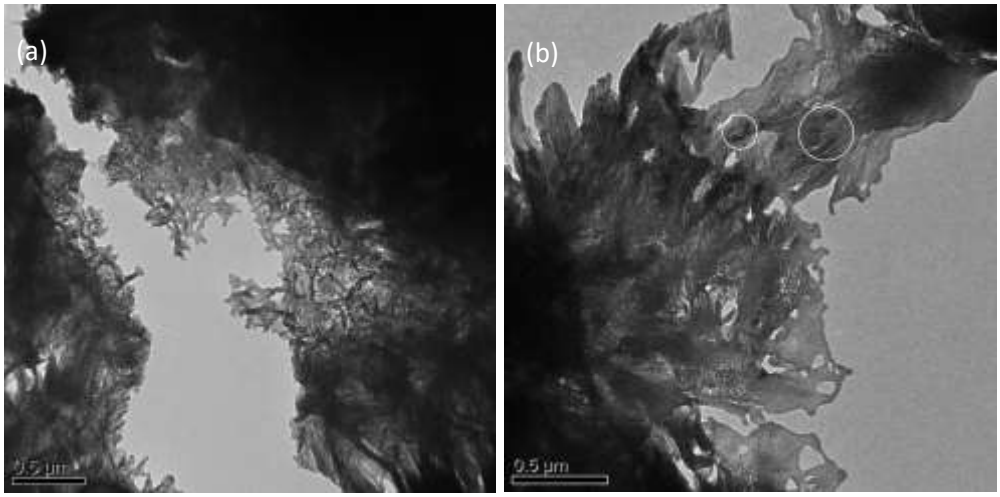

Figure 13. TEM micrographs of 30% GGBS 0.57 (72hr) sample exposed to ambient [CO_2] for 4 days (calcite microcrystals are visible in b).

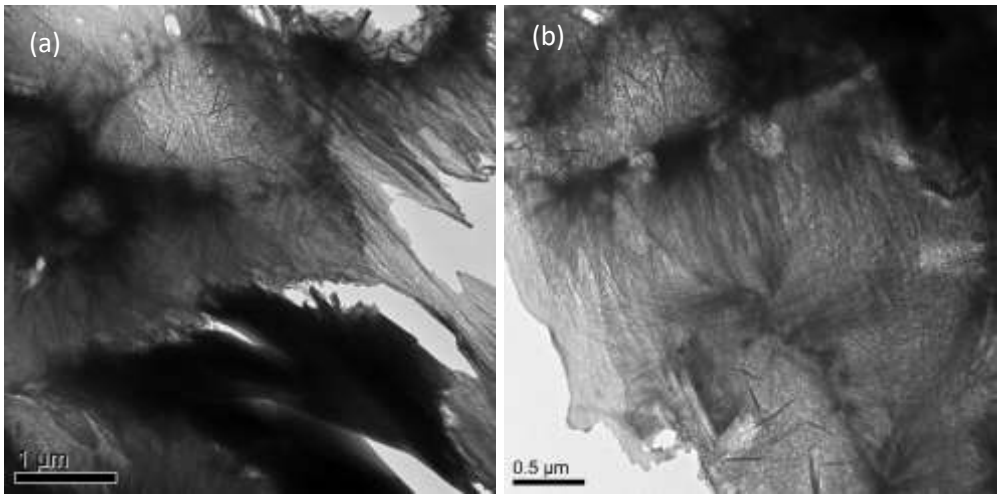

Figure 14. TEM micrographs of 60% GGBS 0.57 (28d) sample exposed to ambient [CO_2] for 2 days.

3.2.2.2 ^{29}Si MAS NMR

Deconvolution data from ^{29}Si NMR spectra are shown in Table 10 for the 0.57 72 hour cured samples following up to 7 days' carbonation. Figure 15 displays the fitted spectra for the 30% slag samples, comparing the t_0 and 4 day carbonated systems. Carbonation always led to loss of Q^1 silicate species and growth in Q^2 sites, reflecting silicate chain polymerisation and increasing mean chain lengths (MCL). This is consistent with calcium abstraction. While

portlandite was present however, silicate polymerisation was modest. Spectra remained dominated by Q^1 species and chain lengths increased only slightly. At 4 days' exposure, portlandite was almost entirely depleted and carbonation increased dramatically, with a marked increase in Q^2 sites and substantially longer silicate chains (MCL 7.9 and 8.2). This considerable change in C-S-H structure coincided with changes seen in ATR-FTIR spectra carbonate content and speciation derived from thermal analysis data.

Table 10. Results from deconvolution of single pulse ^{29}Si NMR spectra for 0.57 – 72hr cured samples following up to 7 days exposure to ambient [CO_2].

				Chemical shifts / δ (ppm)			Relative intensities (%)				Al/Si		
	w/b	t_0	Exposure to CO_2 (d)	Q^1	Q^2(1Al)	Q^2	Q^1	Q^2(1Al)	Q^2	MCL	NMR	TEM [s.d.] Ip	TEM [s.d.] Op
CEM I	0.57	72h	0	-78.75	-81.8	-84.27	74	14	12	2.9	0.07	0.07	0.11 [0.03]
CEM I	0.57	72h	4	-78.84	-81.76	-84.59	59	16	25	3.6	0.08	-	-
CEM I	0.57	72h	7	-79.09	-82.24	-85.15	33	17	50	6.6	0.08	-	-
30% PFA	0.57	72h	0	-78.56	-81.44	-84.11	59	19	22	3.7	0.10	0.11 [0.02]	0.12 [0.05]
30% PFA	0.57	72h	2	-78.88	-82.13	-84.78	51	17	32	4.3	0.09	-	-
30% PFA	0.57	72h	4	-79.14	-82.12	-84.98	29	18	53	7.6	0.09	-	-
30% GGBS	0.57	72h	0	-78.84	-81.68	-84.68	61	22	18	3.7	0.11	0.11	0.16 [0.07]
30% GGBS	0.57	72h	2	-79.07	-82.04	-84.83	48	19	33	4.6	0.09	-	-
30% GGBS	0.57	72h	4	-79.33	-82.3	-85.16	26	18	56	8.2	0.09	0.10 [0.03]	0.09 [0.02]
60% GGBS	0.57	72h	0	-79.11	-81.22	-84.29	38	27	35	6.0	0.13	-	-
60% GGBS	0.57	72h	2	-78.93	-82.32	-85.57	14	22	65	16.1	0.11	-	-

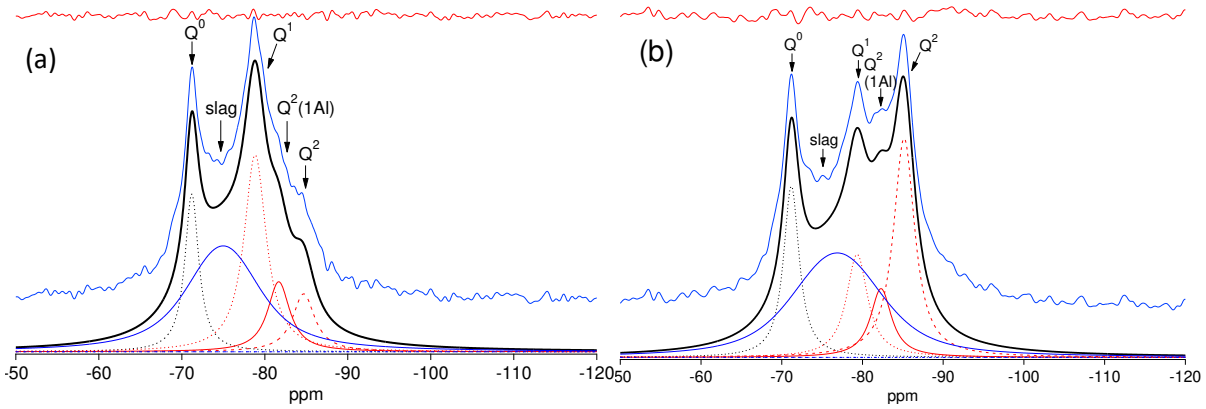

Figure 15. Single pulse ^{29}Si MAS NMR spectra for 30% GGBS 0.57 – 72 hour cured samples (a) t_0 and (b) exposed to ambient [CO_2] for 4 days.

Similar behaviour has been seen from naturally carbonated C_3S pastes [17] and for Ca-rich C-S-H [71]. Sevelsted and Skibsted [48] proposed that upon carbonation of a synthetic C-S-

H sample there is initial decalcification, removing Ca from the interlayer and defect sites until a Ca/Si ratio 0.67 is reached. They observed variations in carbonation behaviour relating resistance to decomposition to higher Ca/Si ratios. A period of gradual decalcification was also reported by Chen *et al*. [22] for leached samples, where accelerated effects only began once Ca/Si ratios of 1.2 and lower had been attained. However, this gradual process did not occur for blended cement (silica fume – WPC), which rapidly decalcified, and was attributed to a low initial Ca/Si ratio (1.35) and almost complete absence of portlandite.

4. Discussion

Improved performance of composite cements over neat Portland cement systems has been widely reported experimentally [3, 4, 6]. This is explained by refinement of the cement microstructure with the transformation from fibrillar to foil-like morphology of Op C-S-H. Foil-like C-S-H fills space with a more finely distributed porosity, reducing interconnectivity and rates of diffusion [1, 2]. However, studies typically investigate well hydrated materials which may not be realistic when considering curing regimes employed in practice.

Within 72 hours clinker hydration in the CEM I system was already considerable and further hydration would primarily include continued C-S-H formation producing finer Op regions as space becomes more constrained [77]. At these early ages C-S-H composition was dominated by Q^1 resonances from alite hydration [78]. Prolonged hydration led to more Q^2 sites and fewer Q^1 sites but little variation was observed for the Q^2(1Al) species, consistent with results from other studies [79, 80]. The proportions of Q^1, Q^2(1Al) and Q^2 sites were similar for equivalent ages regardless of w/b ratio.

The composite systems displayed significant variability depending on curing length, w/b ratio, substitution level and replacement material. While others have reported minimal PFA reaction within the first 7 days, TEM micrographs showing foil-like Op C-S-H and EDX showing a reduced Ca/Si ratio (1.55) confirmed slight fly ash hydration within 72 hours.

620 Subsequent reaction to 28 days was relatively small, evidenced by an average Ca/Si ratio of
621 1.49 following 28 days curing. Meanwhile, the more 30% slag system showed a Ca/Si ratio
622 of 1.39 after just 72 hours, illustrating slag's greater reactivity than PFA.

623 The more gradual hydration of SCMs than clinker may affect durability. Balayssac *et al*. [13]
624 assessed the carbonation depth of Portland cement, limestone (25%) and slag (65%)
625 concretes following varying lengths of curing. Concrete performance improved with longer
626 curing before exposure. However for composite materials, or as cement content decreased,
627 durability improvements were much greater during later periods of curing. For example, for
628 cement content 420kg/m^3 performance increased 50% between 1-3 days curing and 10%
629 between 3-28 days curing, whereas for cement content 300kg/m^3 performance increased
630 10% between 1-3 days and 30% between 3-28 days.

631 Changes in the distribution of Q^1, Q^2(1Al) and Q^2 species in the composite materials became
632 more apparent with time as the SCMs reacted. Higher proportions of Q^2 species are seen as
633 Ca/Si falls [54]. Here, Ca/Si ratios determined by TEM-EDX for 30% replacement systems
634 ranged from 1.39 – 1.55 and Q^1 species were dominant, in line with [47]. For the 60% slag
635 sample (w/b 0.57) cured for 28 days, the Ca/Si ratio was 1.27 and the relative proportions of
636 Q^1 and Q^2 became almost equivalent, resulting in higher calculated chain lengths, confirming
637 the higher degrees of polymerisation expected with increasing slag (or PFA) loading [1, 24,
638 53, 77]. Despite this, the longest MCL was determined to be 6.6, which is relatively low when
639 compared to values determined for blended cements in similar studies. The values
640 determined here reflect the MCL of reasonably young pastes (<28 days) and, as with the
641 neat systems, chain lengths are expected to increase as hydration proceeds.

642 Phase assemblage predictions for the slag systems compare well with modelled data [23].
643 The portlandite content is predicted to decrease with increasing replacement, but remain
644 present up to much higher levels of substitution (<65%) compared with equivalent fly ash
645 composites, even at considerable levels of reaction (75%). Calculations predict
646 monocarboaluminate formation over monosulfate, with decreased quantities of AFt and

647 increased quantities of hydrotalcite formed with increasing replacement levels. Generally
648 experimental studies show lower amounts of AFt and AFm in slag cements compared to
649 neat systems, resulting from greater uptake of Al in C-S-H [24, 33, 81]. However, in this
650 study, thermodynamic equilibrium had not been attained. Consequently, the results (Figures
651 S-1 and S-3) suggest enhanced formation of AFm phases for the slag systems compared
652 with the CEM I sample. The hydration of C_3A was rapid for all the systems with almost
653 complete reaction within 72 hours (data not shown) indicating a contribution of Al from the
654 slag, as seen elsewhere [36]. Increased degrees of reaction were measured for the GGBS in
655 these systems at both replacement levels, suggesting that the slag is a source of Al for
656 increased AFm precipitation.

657 Thermodynamic calculations presented by Lothenbach *et al*. [23] for replacement of Portland
658 cement by PFA predict complete consumption of portlandite at substitution levels of 30%.
659 Here, considerable quantities of portlandite were always measured however, due to the low
660 degree reaction of fly ash. Lothenbach *et al*. [23] assumed 50% reaction of the fly ash,
661 significantly greater than in this study. This is also significantly larger than that measured
662 elsewhere at 28 days hydration, Ben Haha *et al*. [41] measured a degree of PFA hydration of
663 21% for a 35% PFA sample and Kovacs [42] measured 10-12% for a 40% PFA system.
664 Increased AFm and decreased AFt contents are in good agreement with the modelled
665 calculations and with experimental studies in the literature [26, 35, 82]. Enhanced aluminate
666 availability without corresponding increases in sulphate contents favours the formation of
667 AFm species over AFt, as seen here where the degree of fly ash hydration was higher (i.e.
668 at t_0 28d and w/b ratio 0.57). Dyer and Dhir [83] reported similar findings with conversion of
669 AFt to monosulfate upon fly ash replacement, concluding that small increases in the total AFt
670 and AFm contents with increasing PFA content were due to a contribution from the
671 replacement material.

672 Thiery et al. [19] stated that carbonation kinetics, principally of portlandite, was the rate
673 determining process, rather than CO_2 diffusion when considering carbonation of CEM I

674 systems. The hydration of Portland cement is still substantial at early ages, and although
675 differences in porosity and permeability will exist with different curing lengths and w/c ratios,
676 these will not be as great as seen for blended cements, being further exaggerated at very
677 short curing durations and as w/b ratio and replacement increase. In highly porous systems,
678 portlandite availability will govern the rate and extent of carbonation, as seen for the 0.57 -
679 72 hour cured samples. However, comparing the 30% slag systems cured for either 72
680 hours or 28 days indicated this is not always the case for composite materials. Both systems
681 had equivalent portlandite contents at t_0, but after 7 days' exposure to ambient CO_2,
682 portlandite had been completely consumed in the sample cured for 72 hours, and
683 decalcification of the other Ca bearing hydrate phases was substantial. At the same
684 exposure age, the sample cured for 28 days still contained portlandite, and so carbonate
685 produced from the other phases (C-S-H, AFt, AFm) was reduced by 50%. In the mature
686 paste, despite the same initial portlandite content, its accessibility is substantially reduced
687 due to the enhanced microstructure, slowing CO_2 diffusion. In mature systems both the
688 kinetics of carbonation and the diffusion of CO_2 play a role, but in immature pastes porosity
689 increases and resistance to carbonation becomes reliant on the chemical kinetics. This has
690 implications for the surfaces of improperly cured blended materials in which reduced
691 portlandite contents are expected and where microstructures may permit ready ingress of
692 CO_2.

693 Carbonation of AFm phases occurred almost immediately upon exposure to CO_2. In the
694 presence of portlandite, there was conversion of monosulphate to a mixture of hemi- and
695 monocarboaluminate. But in the absence of portlandite, there was rapid decomposition of
696 the AFm phases, with the carbonation of AFt producing gypsum as a decomposition product
697 (as for the 0.57 72hr cured 60% GGBS system).

698 The mechanism of AFt carbonation shows an induction period during which decomposition
699 of AFt is minimal [61]. This induction period is related to saturation and dissolution of the
700 phase, effectively raising the pH of the environment and enhancing the carbonation kinetics

by more rapid dissolution of CO_2. AFt degradation then forms gypsum, vaterite, alumina gel and water. Typically, increased carbonation following the depletion, or inaccessibility, of portlandite are only discussed in relation to C-S-H. Here, the same concept can also be applied to calcium aluminate phases. Highly alkaline pore solutions promote dissociation of carbonic acid ($HCO_3^- + H^+$) and portlandite dissolution is very fast, being thermodynamically favoured over C-S-H [84]. While Ca is supplied by portlandite, relatively little decalcification of the other phases occurs. Once portlandite is no longer able to supply Ca^{2+} ions to solution, Ca is provided by the remaining phases and carbonation rates increase. The solubility of portlandite therefore prevents significant decomposition of all the Ca bearing hydrate phases, not just C-S-H.

Many studies describe simultaneous carbonation of portlandite and C-S-H, assigning additional $CaCO_3$ contents to that produced from portlandite solely to C-S-H [19, 60]. Here we show that AFm phases are involved in the very early reactions, even under ambient conditions, contributing to the production of carbonate species. XRD data indicated minimal change in AFt composition.

Differences in carbonation behaviour observed following short periods of curing at high (0.57) and low (0.40) w/b ratios emphasises the effect of porosity, particularly for composite cements. Higher w/b ratios encouraged early-age hydration, leading to increased portlandite contents and increasing carbonation resistance. However the high porosity of underdeveloped microstructures, as expected at early ages for slower reacting SCM materials, allows ready CO_2 diffusion, resulting in greater carbonation. As the w/b ratio is reduced, porosity and diffusion rates are also greatly reduced, and both carbonation kinetics and porosity become important determinants. Kim et al. [85] showed a 192% increase in air permeability for Portland cement mortars as w/c ratios were increased from 0.45 to 0.60. High cement replacement levels will also result in high porosities, as reported by Hill and Sharp [86] for slag cement pastes. This is demonstrated here, where reduced w/b ratios

727 were unable to mitigate the effects of high levels of replacement (60% GGBS) to the same
728 degree as for materials with moderate replacement levels (30%).

729

730 **5. Conclusions**

731 The early-age carbonation reactions of cement pastes are controlled by both chemical
732 kinetics and paste porosities. High w/b ratios and short curing periods have open and
733 underdeveloped microstructures, exacerbated in composite materials, in which CO_2 is
734 permitted to diffuse easily. Portlandite availability becomes the rate determining factor. With
735 prolonged curing or decreased w/b ratio both carbonation kinetics and system porosity
736 control carbonation. Low w/b ratios can hinder carbonation following short curing periods at
737 moderate substitution levels, but not at higher replacement levels.

738 In the presence of portlandite, there is minor carbonation of all other Ca bearing hydrate
739 phases. However, once portlandite is consumed, decalcification is more aggressive. Both Ca
740 and Al are removed from C-S-H gel, with significant increases in silicate polymerisation.
741 Thermal analysis gives a clear indication of amorphous calcium carbonate formation.
742 Subsequently, calcite or vaterite microcrystals form in Op regions, while Ca is removed from
743 Ip regions with no visual change in the microstructure, suggesting carbonation shrinkage.

744 Carbonation of the AFm phases occurred in 2 stages. During early stages of carbonation,
745 AFm phases transforming from monosulfoaluminate to hemi- and monocarboaluminate
746 before complete decalcification. Portlandite can prevent AFt and AFm decomposition, but
747 the absence of portlandite leads to decomposition of these phases during carbonation.

748 Reduced w/b ratios improve carbonation resistance following both short and prolonged
749 curing, due to significantly reduced porosity. However, lower water contents cannot mitigate
750 the effects of high levels of replacement (60% GGBS) following short curing periods, to the
751 same degree as for materials with moderate substitution (30%).

752

Acknowledgements

This work was funded and supported by Nanocem (nanocem.org).

References

1. Richardson, I.G. and G.W. Groves, *Microstructure and microanalysis of hardened cement pastes involving ground granulated blast-furnace slag.* Journal of Materials Science, 1992. **27**(22): p. 6204-6212.
2. Scrivener, K.L. and A. Nonat, *Hydration of cementitious materials, present and future.* Cement and Concrete Research, 2011. **41**(7): p. 651-665.
3. Bijen, J., *Benefits of slag and fly ash.* Construction and Building Materials, 1996. **10**(5): p. 309-314.
4. Marsh, B.K., R.L. Day, and D.G. Bonner, *Pore structure characteristics affecting the permeability of cement paste containing fly ash.* Cement and Concrete Research, 1985. **15**(6): p. 1027-1038.
5. Al-Amoudi, O., et al., *Performance and Correlation of the Properties of Fly Ash Cement Concrete.* Cement, Concrete and Aggregates, 1996. **18**(2): p. 71-77.
6. Canut, M.M.C., *Pore structure in blended cement pastes.* 2011.
7. Berodier, E. and K. Scrivener, *Evolution of pore structure in blended systems.* Cement and Concrete Research, 2015. **73**: p. 25-35.
8. Idowu, O., Black, L, *The Effect of Improper Curing on Properties That May Affect Concrete Durability.* Magazine of Concrete Research, 2018. **70**(12): p. 633-647.
9. *DIN 1045-3:2012-03. Concrete, reinforced and prestressed concrete structures - Part 3: Execution of structures - Application rules for DIN EN 13670*.
10. *NBN B 15-100 (2008). Methodology for the assessment and the validation of the fitness for use of cements or additions of type II for concrete*.
11. *Conrete library of JSCE NO.28. Recommendation for construction of concrete containing ground granulated blast-furnace slag as an admixture*.
12. Güneyisi, E., et al., *Estimation of chloride permeability of concretes by empirical modeling: Considering effects of cement type, curing condition and age.* Construction and Building Materials, 2009. **23**(1): p. 469-481.
13. Balayssac, J.P., C.H. Détriché, and J. Grandet, *Effects of curing upon carbonation of concrete.* Construction and Building Materials, 1995. **9**(2): p. 91-95.
14. Fraay, A.L.A., J.M. Bijen, and Y.M. de Haan, *The reaction of fly ash in concrete a critical examination.* Cement and Concrete Research, 1989. **19**(2): p. 235-246.
15. Deschner, F., et al., *Hydration of Portland cement with high replacement by siliceous fly ash.* Cement and Concrete Research, 2012. **42**(10): p. 1389-1400.

16. Parrott, L.J., *Damage caused by carbonation of reinforced concrete.* Materials and Structures, 1990. **23**(3): p. 230-234.

17. Groves, G.W., et al., *Progressive Changes in the Structure of Hardened C3S Cement Pastes due to Carbonation.* Journal of the American Ceramic Society, 1991. **74**(11): p. 2891-2896.

18. Richardson, I.G., et al., *The carbonation of OPC and OPC/silica fume hardened cement pastes in air under conditions of fixed humidity.* Advances in Cement Research, 1993. **5**(18): p. 81-86.

19. Thiery, M., et al., *Investigation of the carbonation front shape on cementitious materials: Effects of the chemical kinetics.* Cement and Concrete Research, 2007. **37**(7): p. 1047-1058.

20. Groves, G.W., D.I. Rodway, and I.G. Richardson, *The carbonation of hardened cement pastes.* Advances in Cement Research, 1990. **3**(11): p. 117-125.

21. Ho, D.W.S., Q.Y. Cui, and D.J. Ritchie, *The influence of humidity and curing time on the quality of concrete.* Cement and Concrete Research, 1989. **19**(3): p. 457-464.

22. Chen, J.J., J.J. Thomas, and H.M. Jennings, *Decalcification shrinkage of cement paste.* Cement and Concrete Research, 2006. **36**(5): p. 801-809.

23. Lothenbach, B., K. Scrivener, and R.D. Hooton, *Supplementary cementitious materials.* Cement and Concrete Research, 2011. **41**(12): p. 1244-1256.

24. Taylor, R., I.G. Richardson, and R.M.D. Brydson, *Composition and microstructure of 20-year-old ordinary Portland cement–ground granulated blast-furnace slag blends containing 0 to 100% slag.* Cement and Concrete Research, 2010. **40**(7): p. 971-983.

25. Kocaba, V., E. Gallucci, and K.L. Scrivener, *Methods for determination of degree of reaction of slag in blended cement pastes.* Cement and Concrete Research, 2012. **42**(3): p. 511-525.

26. Luke, K. and E. Lachowski, *Internal Composition of 20-Year-Old Fly Ash and Slag-Blended Ordinary Portland Cement Pastes.* Journal of the American Ceramic Society, 2008. **91**(12): p. 4084-4092.

27. Castellote, M., et al., *Chemical changes and phase analysis of OPC pastes carbonated at different CO2 concentrations.* Materials and Structures, 2009. **42**(4): p. 515-525.

28. Leemann, A., et al., *Relation between carbonation resistance, mix design and exposure of mortar and concrete.* Cement and Concrete Composites, 2015. **62**: p. 33-43.

29. Villain, G., M. Thiery, and G. Platret, *Measurement methods of carbonation profiles in concrete: Thermogravimetry, chemical analysis and gammadensimetry.* Cement and Concrete Research, 2007. **37**(8): p. 1182-1192.

30. Morandeau, A., M. Thiéry, and P. Dangla, *Impact of accelerated carbonation on OPC cement paste blended with fly ash.* Cement and Concrete Research, 2015. **67**: p. 226-236.

31. Zhang, J. and G.W. Scherer, *Comparison of methods for arresting hydration of cement.* Cement and Concrete Research, 2011. **41**(10): p. 1024-1036.

32. Snellings, R., *Chapter 4. X-ray powder diffraction applied to cement in A Practical Guide to Microstructural Analysis of Cementitious Materials*. 2016, Boca Raton, FL 33487-2742: CRC Press Taylor & Francis Group, p 107 - 176.
33. Kocaba, V., *Development and Evaluation of Methods to Follow Microstructural Development of Cementitious Systems Including Slags*. 2009, École Polytechnique Federale de Lausanne.
34. Love, C.A., *Microstructure and silicate anion structure of hardened blended cement pastes*, in *School of Civil Engineering*. 2002, University of Leeds.
35. De Weerdt, K., et al., *Hydration mechanisms of ternary Portland cements containing limestone powder and fly ash.* Cement and Concrete Research, 2011. **41**(3): p. 279-291.
36. Whittaker, M., et al., *The role of the alumina content of slag, plus the presence of additional sulfate on the hydration and microstructure of Portland cement-slag blends.* Cement and Concrete Research, 2014. **66**: p. 91-101.
37. Richardson, I.G., et al., *Hydration of water- and alkali-activated white Portland cement pastes and blends with low-calcium pulverized fuel ash.* Cement and Concrete Research, 2016. **83**: p. 1-18.
38. Whittaker, M., *The Impact of Slag Composition on the Microstructure of Composite Slag Cements Exposed to Sulfate Attack*. 2014, Uinversity of Leeds.
39. Luke, K. and F.P. Glasser, *Internal chemical evolution of the constitution of blended cements.* Cement and Concrete Research, 1988. **18**(4): p. 495-502.
40. Lumley, J.S., et al., *Degrees of reaction of the slag in some blends with Portland cements.* Cement and Concrete Research, 1996. **26**(1): p. 139-151.
41. Haha, M.B., K. De Weerdt, and B. Lothenbach, *Quantification of the degree of reaction of fly ash.* Cement and Concrete Research, 2010. **40**(11): p. 1620-1629.
42. Kovács, R., *Effect of the hydration products on the properties of fly-ash cements.* Cement and Concrete Research, 1975. **5**(1): p. 73-82.
43. Matschei, T., B. Lothenbach, and F.P. Glasser, *The AFm phase in Portland cement.* Cement and Concrete Research, 2007. **37**(2): p. 118-130.
44. Skibsted, J., E. Henderson, and H.J. Jakobsen, *Characterization of calcium aluminate phases in cements by aluminum-27 MAS NMR spectroscopy.* Inorganic Chemistry, 1993. **32**(6): p. 1013-1027.
45. Andersen, M.D., H.J. Jakobsen, and J. Skibsted, *Incorporation of Aluminum in the Calcium Silicate Hydrate (C−S−H) of Hydrated Portland Cements: A High-Field 27Al and 29Si MAS NMR Investigation.* Inorganic Chemistry, 2003. **42**(7): p. 2280-2287.
46. Skibsted, J. and H.J. Jakobsen, *Characterization of the calcium silicate and aluminate phases in anhydrous and hydrated Portland cements in Nuclear Magnetic Resonance Spectroscopy of Cement-Based Materials, pp3 -45*. 1998.
47. Andersen, M.D., H.J. Jakobsen, and J. Skibsted, *A new aluminium-hydrate species in hydrated Portland cements characterized by 27Al and 29Si MAS NMR spectroscopy.* Cement and Concrete Research, 2006. **36**(1): p. 3-17.

48. Sevelsted, T.F. and J. Skibsted, *Carbonation of C–S–H and C–A–S–H samples studied by 13C, 27Al and 29Si MAS NMR spectroscopy.* Cement and Concrete Research, 2015. **71**: p. 56-65.

49. Groves, G.W., P.J. Le Sueur, and W. Sinclair, *Transmission Electron Microscopy and Microanalytical Studies of Ion-Beam-Thinned Sections of Tricalcium Silicate Paste.* Journal of the American Ceramic Society, 1986. **69**(4): p. 353-356.

50. Richardson, I.G. and G.W. Groves, *Microstructure and microanalysis of hardened ordinary Portland cement pastes.* Journal of Materials Science, 1993. **28**(1): p. 265-277.

51. Richardson, I.G., *The nature of the hydration products in hardened cement pastes.* Cement and Concrete Composites, 2000. **22**(2): p. 97-113.

52. Richardson, I.G., *Electron microscopy of cements Chapter 22 in Structure and Performance of Cements, 2nd edition*, ed. B. Barnes and J. Bensted. 2002: Spon Press, p 500-556.

53. Girão, A.V., et al., *Composition, morphology and nanostructure of C–S–H in 70% white Portland cement–30% fly ash blends hydrated at 55 °C.* Cement and Concrete Research, 2010. **40**(9): p. 1350-1359.

54. Rodriguez, E.T., *Relation between composition, structure and morphology in C-S-H*, in *School of Civil Engineering* 2015, The University of Leeds.

55. Richardson, I.G., et al., *Characterisation of cement hydrate phases by TEM, NMR and Raman spectroscopy.* Advances in Cement Research, 2010. **22**(4): p. 233-248.

56. Magi, M., et al., *Solid-state high-resolution silicon-29 chemical shifts in silicates.* The Journal of Physical Chemistry, 1984. **88**(8): p. 1518-1522.

57. Cong, X. and R.J. Kirkpatrick, *29Si MAS NMR study of the structure of calcium silicate hydrate.* Advanced Cement Based Materials, 1996. **3**(3–4): p. 144-156.

58. Richardson, I.G., et al., *Location of Aluminum in Substituted Calcium Silicate Hydrate (C-S-H) Gels as Determined by 29Si and 27Al NMR and EELS.* Journal of the American Ceramic Society, 1993. **76**(9): p. 2285-2288.

59. Richardson, I.G., et al., *The characterization of hardened alkali-activated blast-furnace slag pastes and the nature of the calcium silicate hydrate (C-S-H) phase.* Cement and Concrete Research, 1994. **24**(5): p. 813-829.

60. Borges, P.H.R., et al., *Carbonation of CH and C-S-H in Composite Cement Pastes Containing High Amounts of BFS.* Cement and Concrete Research, 2010. **40**: p. 284 - 292.

61. Zhou, Q. and F.P. Glasser, *Kinetics and mechanism of the carbonation of ettringite.* Advances in Cement Research, 2000. **12**(3): p. 131-136.

62. Fernández-Carrasco, L., D. Torréns-Martín, and S. Martínez-Ramírez, *Carbonation of ternary building cementing materials.* Cement and Concrete Composites, 2012. **34**(10): p. 1180-1186.

63. Shi, Z., et al., *Experimental studies and thermodynamic modeling of the carbonation of Portland cement, metakaolin and limestone mortars.* Cement and Concrete Research, 2016. **88**: p. 60-72.

64. Lothenbach, B., et al., *Influence of limestone on the hydration of Portland cements.* Cement and Concrete Research, 2008. **38**(6): p. 848-860.

65. Zajac, M., et al., *Influence of limestone and anhydrite on the hydration of Portland cements.* Cement and Concrete Composites, 2014. **46**: p. 99-108.

66. Nishikawa, T., et al., *Decomposition of synthesized ettringite by carbonation.* Cement and Concrete Research, 1992. **22**(1): p. 6-14.

67. Li, S., *Carbonation of 20-year-old Blended Cement Pastes*. 2011, The University of Leeds.

68. Šauman, Z., *Carbonization of porous concrete and its main binding components.* Cement and Concrete Research, 1971. **1**(6): p. 645-662.

69. Slegers, P.A. and P.G. Rouxhet, *Carbonation of the hydration products of tricalcium silicate.* Cement and Concrete Research, 1976. **6**(3): p. 381-388.

70. Dubina, E., et al., *Influence of water vapour and carbon dioxide on free lime during storage at 80 °C, studied by Raman spectroscopy.* Spectrochimica Acta Part A: Molecular and Biomolecular Spectroscopy, 2013. **111**: p. 299-303.

71. Black, L., et al., *Structural Features of C–S–H(I) and Its Carbonation in Air—A Raman Spectroscopic Study. Part II: Carbonated Phases.* Journal of the American Ceramic Society, 2007. **90**(3): p. 908-917.

72. Ylmén, R. and U. Jäglid, *Carbonation of Portland Cement Studied by Diffuse Reflection Fourier Transform Infrared Spectroscopy.* International Journal of Concrete Structures and Materials, 2013. **7**(2): p. 119-125.

73. Yu, P., et al., *Structure of Calcium Silicate Hydrate (C-S-H): Near-, Mid-, and Far-Infrared Spectroscopy.* Journal of the American Ceramic Society, 1999. **82**(3): p. 742-748.

74. Anderson, F.A. and L. Brečević, *Infrared spectra of amorphous and crystalline calcium carbonate.* Acta Chemica Scandinavica, 1991. **45**: p. 1018 - 1024.

75. Fernández-Carrasco, L. and E. Vázquez, *Reactions of fly ash with calcium aluminate cement and calcium sulphate.* Fuel, 2009. **88**(9): p. 1533-1538.

76. Ylmén, R., et al., *Early hydration and setting of Portland cement monitored by IR, SEM and Vicat techniques.* Cement and Concrete Research, 2009. **39**(5): p. 433-439.

77. Taylor, R., I.G. Richardson, and R.M.D. Brydson, *Nature of C–S–H in 20 year old neat ordinary Portland cement and 10% Portland cement–90% ground granulated blast furnace slag pastes.* Advances in Applied Ceramics, 2007. **106**(6): p. 294-301.

78. Hirljac, J., Z.Q. Wu, and J.F. Young, *Silicate polymerization during the hydration of alite.* Cement and Concrete Research, 1983. **13**(6): p. 877-886.

79. Andersen, M.D., H.J. Jakobsen, and J. Skibsted, *Characterization of white Portland cement hydration and the C-S-H structure in the presence of sodium aluminate by 27Al and 29Si MAS NMR spectroscopy.* Cement and Concrete Research, 2004. **34**(5): p. 857-868.

80. Lippmaa, E., et al., *A high resolution 29Si NMR study of the hydration of tricalciumsilicate.* Cement and Concrete Research, 1982. **12**(5): p. 597-602.

81. Richardson, I.G. and G.W. Groves, *The structure of the calcium silicate hydrate phases present in hardened pastes of white Portland cement/blast-furnace slag blends.* Journal of Materials Science, 1997. **32**(18): p. 4793-4802.

82. Escalante-Garcia, J.I. and J.H. Sharp, *The chemical composition and microstructure of hydration products in blended cements.* Cement and Concrete Composites, 2004. **26**(8): p. 967-976.

83. Dyer, T.D. and R.K. Dhir, *Hydration reactions of cement combinations containing vitrified incinerator fly ash.* Cement and Concrete Research, 2004. **34**(5): p. 849-856.

84. Morandeau, A., M. Thiéry, and P. Dangla, *Investigation of the carbonation mechanism of CH and C-S-H in terms of kinetics, microstructure changes and moisture properties.* Cement and Concrete Research, 2014. **56**: p. 153-170.

85. Kim, Y.-Y., et al., *Effect of W/C Ratio on Durability and Porosity in Cement Mortar with Constant Cement Amount.* Advances in Materials Science and Engineering.Volume 2014 (2014), Article ID 273460, 11 pages.

86. Hill, J. and J.H. Sharp, *The mineralogy and microstructure of three composite cements with high replacement levels.* Cement and Concrete Composites, 2002. **24**(2): p. 191-199.